EES Solar

Accepted Manuscript

This article can be cited before page numbers have been issued, to do this please use: L. Liu, W. Li, S. Liu, X. Lu and J. Yan, *EES Sol.*, 2026, DOI: 10.1039/D5EL00216H.

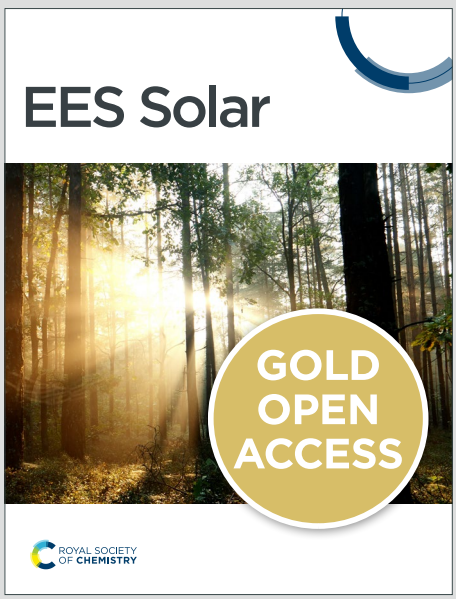

View Article Online
DOI: 10.1039/D5EL00216H

The classical Marcus theory serves as a standard framework for experimentally determining the properties of charge transfer states in organic photovoltaics. Although it has been highly successful for traditional systems with large energy offsets, it encounters significant limitations when applied to state-of-the-art non-fullerene acceptor-based systems. Here, we provide a detailed critique of potential issues and errors arising from the application of classical Marcus analysis. We also propose practical guidelines for more accurately estimating charge transfer state properties in complex systems—such as those exhibiting large static disorder or spectral overlap among excited states. Furthermore, this work introduces a computational toolkit to facilitate reliable Classical Marcus analysis when charge transfer states are spectroscopically resolvable.

View Article Online
DOI: 10.1039/D5EL00216H

The complexity of Classical Marcus analysis for charge transfer state in organic photovoltaics

Liming Liu[1], Weitang Li[1], Sha Liu[2], Xinhui Lu[3], Jun Yan[1,]*

[1] Guangdong Basic Research Center of Excellence for Aggregate Science, School of Science and Engineering, The Chinese University of Hong Kong (Shenzhen), Longgang, Shenzhen, Guangdong, 518172, P.R. China

[2] Dongguan Key Laboratory of Interdisciplinary Science for Advanced Materials and Large-Scale Scientific Facilities, School of Physical Sciences, Great Bay University, Dongguan, Guangdong, 523000, P. R. China.

[3] Department of Physics, The Chinese University of Hong Kong, New Territories, Hong Kong SAR 999077, China

Corresponding author: yanjun@cuhk.edu.cn

Abstract

Classical Marcus theory is widely used in organic photovoltaics (OPVs) to extract charge transfer (CT) state properties from electroluminescence (EL) and sensitive external quantum efficiency (s-EQE) spectra. However, practical donor-acceptor blends often exhibit complications such as overlap between CT and localized exciton (LE) emissions, large static energetic disorder, and weak CT oscillator strengths, all of which can limit the accuracy of simple Marcus analysis. This article discusses those issues in detail and provides a practical guide to Marcus-based CT analysis for complex cases with invisible CT states and large static disorder. An open-source Python package is released to enable semi-automated Classical Marcus analysis when CT is clearly visible.

View Article Online
DOI: 10.1039/D5EL00216H

Introduction

Electron transfer is a fundamental process in chemistry, physics and biology, underpinning phenomena ranging from photosynthesis to energy conversion devices[1-7]. A modern quantitative description of this process began with the pioneering work of Rudolph Arthur Marcus in the mid-1950s. Since 1956, Marcus proposed a theoretical framework in a series of papers[8-14], which realized the quantitative description of the electron transfer reaction rate for the first time, known as Marcus theory. This theory is applicable to the reaction system without chemical bond formation or cleavage, and the free energy of the system is expressed as a function of the collective nuclear coordinates, which replaces the application of Eyring's transition state theory in this kind of reaction[10].

In the Classical Marcus theory, the initial state (donor-acceptor pair, $D - A$) and the final state (ion pair, $D^- - A^+$) are represented by two intersecting parabolic potential energy surfaces, respectively[15, 16]. The electron transfer rate depends on the energy barrier height at the intersection of these two curves[17]. This process involves two key parameters: one is the difference in Gibbs free energy ΔG^0 of the reaction, which reflects the thermodynamic driving force; the second is the reorganization energy λ, which represents the energy required to adjust the nuclear configuration of the reactant (including the surrounding solvent or medium) to the product state without electron transfer. This description follows from the Franck-Condon principle[18, 19], which states that electron transfer occurs on a time scale much faster than nuclear motion, i.e. the Born-Oppenheimer approximation.

One of the most striking and counterintuitive predictions of the Marcus model is the "inverted region" phenomenon[9]. The general chemical intuition believes that the reaction rate increases with the increase of thermodynamic driving force. However, Marcus theory points out that for high driving force reactions (i.e., $-\Delta G^0 > \lambda$), further increase in the driving force will lead to a reduction in the rate. The experimental verification of the inversion region not only strongly supports the core hypothesis of the theory, but also provides an important basis for understanding the nonradiative transitions with large energy separation between initial and final states in organic optoelectronic devices[20-23].

Marcus theory was originally established for the outer electron transfer reaction in polar solvents. In this model, the reorganization of solvent continuum is the main source of energy barrier. In organic semiconductors, the charge transfer environment includes both low-frequency lattice vibrations and high-frequency intramolecular vibration modes. Since the vibrational energy of many molecules is higher than the thermal energy (k_BT) at room temperature, they must be treated by quantum mechanics[24]. This demand promoted the development of the semi-classical Marcus-Levich-Jortner (MLJ) theory[2], in which electron transfer can occur not only through

View Article Online
DOI: 10.1039/D5EL00216H

thermal activation, but also through the nuclear tunneling effect mediated by the overlap of vibrational wave functions. This extension makes the electron transfer theory more suitable for solid-state systems and is of key significance[25-27].

In organic photovoltaics (OPVs), Marcus theory has gradually developed from a predictive framework of reaction rate to a key diagnostic tool. The performance of OPV devices largely depends on the open circuit voltage (V_{oc}), which is mainly limited by the energy loss in the process of photon-to-electricity conversion[28, 29]. The core of this process lies in the donor-acceptor interface: upon photon absorption, excitons are generated and subsequently dissociate to form a charge transfer (CT) state at the interface[30, 31]. Therefore, CT state is the key intermediate state for charge generation and recombination[32-34], and its energy (E_{CT}) is closely related to the thermodynamic limit for V_{oc} and needs to be accurately measured. Vandewal et al. pioneered the measurements of CT states via simultaneously fitting sensitive external quantum efficiency (s-EQE) and electroluminescence (EL) spectrum using the classical Marcus theory in the high temperature limit with an assumption that the molecular vibrational energy is much lower than the thermal energy k_BT[30, 35]. In this method, CT absorption and emission spectra can be fitted by two symmetric Gaussian functions, eventually E_{CT} and λ can be extracted. This method is now routinely employed in OPV research.

Although the analysis based on the Classical Marcus theory has achieved remarkable success in OPVs, its employment in current high-performance devices faces severe challenges. With the emergence of non-fullerene acceptors (NFAs), the device efficiency has been increased to over 20%, mainly due to a significant reduction in energetic offset and subsequently voltage loss[36-41]. Small offsets also lead to spectra overlap between locally excited (LE) and CT emissions; hence, the standard single-state Marcus analysis is subject to the overlapping interference of many complex factors. Consequently, the weak CT absorption signal is often masked by the steep absorption edge of the narrow band gap NFA, and the EL spectrum is dominated by the bright LE emission[42-44]. If the standard analysis method is directly applied to such spectra, the extracted value of E_{CT} would be close to E_{LE} and overestimated.

In addition, in the system with small energetic offset and strong electronic coupling, LE and CT states may be mixed to form hybrid states that do not conform to the simple Marcus model[45, 46]. This hybridization between LE and CT states creates mixed electronic character that violates Marcus theory's discrete two-state model[47-49]. The degree of this hybridization depends on the ratio of electronic coupling strength to driving force: systems with moderate coupling strength and high driving force have a limited degree of hybridization (about 3%), while in systems where the driving force is close to zero, the hybridization effect is much more significant[47]. The LE-CT hybridization with mixed energy states fundamentally challenges Marcus theory. A three-state vibrational electron model that considers the coupling of electrons and vibrations with localized absorption states is crucial for reliably describing optical

View Article Online
DOI: 10.1039/D5EL00216H

absorption characteristics, because the classical Marcus model leads to incorrect interpretation[48]. This hybridization results an intensity borrowing mechanism that increases the oscillator strength of the effective CT to the ground state, hence suppressing nonradiative voltage losses, which cannot be explained by the classical Marcus theory alone[49].

Finally, the organic semiconductor film itself has significant static energetic disorder, which further complicates the extraction of CT state properties[50-52]. The static disorder caused by irregular molecular packing and conformational changes in organic films leads to a distribution of CT state energies. Intermolecular interactions in organic blends exhibit weak cohesion through van der Waals forces, and combined with conformational irregularities, this results in a broadened distribution of charge transfer states[53]. Static energetic disorder is expected to be pronounced in amorphous organic semiconductors and in heterogeneous blended films commonly used in OPV devices[54]. However, classical Marcus theory assumes the existence of a single charge transfer energy level, with the broadening of its spectral features attributed solely to electron-phonon coupling (dynamic disorder)[55]. Although traditional models can be extended to account for this phenomenon, the commonly applied classical Marcus approach neglects this effect.

In view of the above limitations and challenges, a practical guide on classical Marcus theory analysis of CT states is urgently needed in OPVs. If the existing model is directly applied without fully understanding its premise, it is easy to draw wrong conclusions. The purpose of this study is to first systematically integrate potential problems in classical Marcus analysis, and provide a unified diagnostic framework to elucidate how to carefully interpret the EL and s-EQE spectra under the framework of classical Marcus theory, and pay special attention to static disorder and the mixed LE and CT emission, in particular the invisible CT states in the current NFA-based system.

Basics of classical Marcus theory

Marcus theory provides a framework for calculating the electron transfer rate between two electronic states coupled to a dynamic nuclear environment[10]. The model takes into account the effects of intramolecular vibrations and surrounding molecular matrices. The core is that electron transfer is most likely to occur when the nuclear coordinate fluctuates to a configuration where the initial and final electron energies are equal, a.k.a. vertical transition. This condition conforms to the Franck-Condon principle and the electron transition is much faster than the nuclear motion[18, 19]. The theory uses the non-adiabatic potential energy surface to describe this process. It approximates the potential energy surface of the initial state and the final state to a simple harmonic potential with the same curvature. This parabolic approximation simplifies the geometry of the complex, multi-dimensional and possibly anharmonic

potential energy surface in the real world. The key assumptions are as follows: first of all, the potential energy surface of the initial state and the final state have a quadratic dependence on the nuclear reaction coordinate; secondly, the response of the surrounding environment to charge rearrangement is linear, and the dielectric response changes proportionally. Thirdly, using the Condon approximation, it is assumed that the electron coupling matrix element H_{DA} is independent of the nuclear coordinates, so the transition probability is completely determined by the nuclear configuration. Finally, the model is applicable to the non-adiabatic limit (weak electronic coupling), and the system evolves along the initial potential energy surface until it jumps to the final potential energy surface at the crossover point[24, 56-58]. This hypothesis is particularly consistent with the optically weak transition characteristics of charge transfer states in OPV blends.

For optical transitions involving CT states, it is usually necessary to consider two potential energy surfaces: one represents the ground state (GS) of the D-A pair, and the other represents the CT state ($D^- - A^+$). As shown in **Fig. 1(a)**, these potential energy surfaces are plotted along a generalized one-dimensional "reaction coordinate". Within this parabolic framework, the kinetics and thermodynamics of the charge transfer process are described by several key parameters. For optical transitions of absorption and emission between the ground state and the CT state, the standard Gibbs free energy change ΔG^0 of the reaction is simply the energy difference between the two potential energy surface minima, i.e. the CT state energy E_{CT}. Reorganization energy λ is defined as the energy required to distort the nuclear geometry of the initial state (reactant plus environment) to the equilibrium geometry of the final state without the occurrence of electron transfer event itself. It is the vertical energy difference between the final state potential energy calculated in the equilibrium coordinates of the initial state and the minimum value of the final state potential energy. λ quantifies the energy dissipated by the instantaneous electron transfer when the nuclear coordinates of the system relax to their new equilibrium positions[59-61]. It includes two main contributions: the inner ring component (λ_i) caused by the change of intramolecular bond length and bond angle, and the outer ring component (λ_o) caused by the reorientation of the surrounding polarized medium. In the classical Marcus theory, only the outer reorganization energy is considered[62]. The activation energy $\Delta G^{\ddagger}$ for the transition is the energy of the crossing point of the two parabolas relative to the minimum of the initial state parabola[10]. A straightforward geometric derivation based on the parabolic approximation yields the Marcus equation for the free energy of activation:

$$\Delta G^{\ddagger} = \frac{(\lambda + \Delta G^0)^2}{4\lambda}() \tag{}$$

For the non-radiative recombination process from the CT state back to the ground state, the initial state is the CT state and the final state is the ground state. Therefore,

View Article Online
DOI: 10.1039/D5EL00216H

the driving force is $\Delta G^0 = -E_{CT}$. The activation barrier for this loss pathway is thus given by:

$$\Delta G^{\ddagger}_{rec} = \frac{(\lambda - E_{CT})^2}{4\lambda}()$$

Under the non-adiabatic limit and low frequency approximation, the rate of electron transfer (k_{ET}) is described by the classical Marcus expression:

$$k_{ET} = \frac{2\pi}{\hbar}|H_{DA}|^2 \frac{1}{\sqrt{4\pi\lambda k_B T}} exp\left(-\frac{(\Delta G^0 + \lambda)^2}{4\lambda k_B T}\right)()$$

Where $\hbar$ is the reduced Planck constant, $|H_{DA}|$ is the electronic coupling matrix element, k_B is the Boltzmann constant, and T is the absolute temperature. This quadratic dependence of the activation energy on ΔG^0 leads to the existence of a "normal" and an "inverted" region for reaction rates, suggesting that very large E_{CT} values could potentially suppress non-radiative recombination rates.

The processes of photon absorption and emission are visualized as vertical Franck-Condon transitions on the potential energy diagram. The absorption process involves a vertical transition from the equilibrium configuration (minimum) of the ground state parabola. This transformation terminates on the parabola of the CT state, and its energy is one λ longer than the minimum value of the CT state potential energy surface. Conversely, radiative recombination (emission) involves a vertical transition from the minimum of the CT state parabola down to the ground state parabola. Thus, the energy of the photon corresponding to the maximum absorption and emission intensity are approximately given by:

$$E_{abs} \approx E_{CT} + ()$$

$$E_{em} \approx E_{CT} - ()$$

The energy difference between the absorption and emission maxima is known as the Stokes shift, which provides an experimentally accessible spectroscopic handle for determining the reorganization energy:

$$\text{Stokes Shift} = E_{\text{abs}} - E_{\text{em}} \approx ()$$

These key parameters correspond to EL and s-EQE data (reduced) fitted using the standard Marcus theory, as shown in **Fig. 1(b)**.

In the high temperature limit, when the thermal energy ($k_B T$) is large relative to the energy of the relevant nuclear vibration mode ($\hbar\omega$), the thermal population of the initial vibrational energy levels leads to the Gaussian broadening of the optical transition[30, 35]. Therefore, the absorption $A(E)$ and emission $N(E)$ line shapes will be Gaussian centered on E_{abs} and E_{em}, respectively:

View Article Online
DOI: 10.1039/D5EL00216H

$$A(E) \propto E\ exp\left(-\frac{\left(E-(E_{CT}+\lambda)\right)^2}{4\lambda k_B T}\right) \quad (1)$$

$$N(E) \propto E^3\ exp\left(-\frac{\left(E-(E_{CT}-\lambda)\right)^2}{4\lambda k_B T}\right) \quad (2)$$

Standard Procedure of Marcus analysis

Marcus analysis requires simultaneous investigation of the absorption and emission spectra of the CT state. The theoretical basis of this method is derived from the detailed balance principle under thermal equilibrium conditions: in the thermal equilibrium state, the forward rate of any microscopic process is equal to its reverse rate. For optical transitions, this principle establishes a relationship between the absorption and emission spectrum, which was originally proposed by Kennard and Stepanov[63, 64]. In the context of a solar cell, this principle is formalized in an electro-optical reciprocity relation, which connects the device's photovoltaic quantum efficiency (EQE_{PV}) to its electroluminescence emission photon flux density (ϕ_{em})[65, 66]:

$$\phi_{em}(E) = EQE_{PV}(E) \cdot \phi_{BB}(E,T)\left[exp\left(\frac{qV}{kT}\right)-1\right] \quad (3)$$

where $\phi_{BB}(E,T)$ is the spectral flux density of a blackbody radiator at absolute temperature T, and V is the applied voltage. This equation elegantly links the process of absorbing a photon to generate an electron-hole pair (probed by EQE_{PV}, assuming $EQE_{PV} \approx A(E)$) with the reverse process of an electron-hole pair recombining to emit a photon (probed by $N(E)$[50], i.e. the number of photons collected for a given time duration and device area, hence $N(E) \propto \phi_{em}(E)$).

For the analysis, the highly sensitive $EQE_{PV}(E)$ spectrum and EL intensity spectrum $N(E)$ of the solar cell device are first carefully measured. Once obtained, the reduced absorption spectrum is calculated by dividing the measured EQE_{PV} by the photon energy E resulting in a quantity proportional to the absorption cross-section:

$$red.EQE_{PV}(E) = \frac{EQE_{PV}(E)}{E} \quad (4)$$

Similarly, reduced emission spectrum is mirrored to the reduced absorption spectrum:

$$red.EL(E) = \frac{N(E)}{E^3} \quad (5)$$

The manual fitting process requires judgment of visual features such as curve trend,

peak position and line width, and normalization of $red.EQE_{PV}(E)$ and $red.EL(E)$ is required. After this processing, the two reduced spectra are ready for quantitative fitting, as depicted in **Fig. 2(a)**.

In large offset case, the CT absorption and emission characteristics can be clearly separated from the LE transition in the spectrum, showing obvious peaks or tails in the sub-band gap region, as shown in **Fig. 2(a)**. This spectral separation effectively avoids the complexity caused by the overlap of absorption bands, so that we can directly and clearly fit the characteristics of the CT state. The reduced absorption and emission spectra are then fitted using the Gaussian line shapes derived from the Classical Marcus theory, respectively:

$$\text{red. } EQE_{PV}(E) = \frac{A}{\sqrt{4\pi\lambda k_B T}} \cdot \exp\left(-\frac{\left(E - (E_{CT} + \lambda)\right)^2}{4\lambda k_B T} \right) \quad (1)$$

$$\text{red. } EL(E) = \frac{B}{\sqrt{4\pi\lambda k_B T}} \cdot \exp\left(-\frac{\left(E - (E_{CT} - \lambda)\right)^2}{4\lambda k_B T} \right) \quad (2)$$

Where A and B are independent amplitude scaling factors and proportional to the square of the electronic coupling matrix element.

When performing global fitting on the normalized data, the $\text{red. } EL$ curve is usually shifted downward so that the peak height of $\text{red. } EL$ matches that of the CT peak in the $\text{red. } EQE_{PV}$ curve, and E_{CT} and λ are constrained as shared parameters for absorption and emission line shapes. The position and width of the absorption peak (centered at $E_{CT} + \lambda$) and the emission peak (centered at $E_{CT} - \lambda$) are simultaneously described through a set of self-consistent physical parameters, as shown in **Fig. 2(b)**. This approach takes advantage of the inherent mirror symmetry predicted by the theory, and compared with fitting a single spectrum separately, it can obtain more reliable E_{CT} and λ values. Among them, E_{CT} reflects the energy of the interfacial CT state after relaxation, which is the main factor determining the thermodynamic limit of V_{oc} [67, 68], and non-radiative voltage loss ($V_{loss,nr}$)[22, 69]. λ indicates the extent to which nuclei and electrons reorganize at the donor-acceptor interface after a charge transfer event occurs. Smaller reorganizations are preferred because less energy is lost due to structural relaxation. In addition, smaller λ is often associated with steeper absorption edges, hence less dynamic disorder.

Systems with complex absorption and emission spectra

The absorption and emission spectra of a typical bulk heterojunction (BHJ) OPV is determined by various properties of CT states. In the case of traditional large offset

View Article Online
DOI: 10.1039/D5EL00216H

systems (typically > 0.3 eV), e.g. most fullerene based systems, we can clearly see emissions from CT states, making it straightforward to conduct single-state classical Marcus analysis[30]. However, the state-of-the-art NFA systems often feature a small offset (typically < 0.2 eV), leading to possibilities of thermal repopulation[70] and state hybridization[48, 49]. Besides, organic semiconductors have intrinsic static energetic disorder, that may arise from configurational and packing disorder that are strongly correlated to the nanoscale interpenetrating network of donor and acceptors, as shown in **Fig. 3(a)**. In this part, we will discuss the validity of single-state Marcus analysis when absorption and emission spectra are complex.

We employ a previously developed model framework based on the semi-classical Marcus theory[49, 50, 69, 71] to generate a synthetic database of EQE_{PV} and EL spectra as inputs for the subsequent Marcus analysis (**Error! Reference source not found.**). This model generates spectra with complex features of CT states, including static energetic disorder, state hybridization, dark CT, etc., which allows us to fully explore the accuracy of E_{CT} and λ based on the standard Marcus analysis in the case of complex emission spectra. The framework describes the transitions between the ground state (GS or S_0), the localized exciton (LE or S_1) state and the CT state, as shown in the potential energy surface in **Fig. 3(b)**. Based on the semi-classical Marcus-Levich-Jortner (MLJ) theory, the model decomposes the reorganization energy into low-frequency (λ_o) and high-frequency components (λ_i). The low-frequency components, after classical processing, correspond to solvent/matrix relaxation and low-frequency vibration, while the high-frequency components correspond to the dominant quantum mechanical vibration mode with energy of $\hbar\Omega$[69]. The MLJ expression of the non-radiative rate constant k_{nr} is given by the sum of Franck-Condon weighted densities of states:

$$k_{nr} = \frac{2\pi V_{el}^2}{\hbar\sqrt{4\pi\lambda_o k_B T}} \sum_{m=0}^{\infty}\sum_{n=0}^{\infty} \frac{e^{-S}S^{m-n}n!}{m!} \left[L_n^{m-n}(S)\right]^2 e^{\left\{-\frac{[-\hbar\omega+E_{CT}+\lambda_o+(m-n)\hbar\Omega]^2}{4\lambda_o k_B T}\right\}} e^{-\frac{n\hbar\Omega}{k_B T}}() \quad (300)$$

Here, V_{el}^2 is the electronic coupling between the CT and ground states, $S = \lambda_i/\hbar\Omega$ is the Huang-Rhys factor, *m* and *n* designate the quantum number of the vibrational modes of the final and initial state, respectively, and $L_n^{m-n}(S)$ is the generalized Laguerre polynomial of degree n.

Another key component of this model is the state hybridization between LE and CT states, which becomes significant when the offset between them is small (usually < 0.2 eV)[49]. This interaction is mediated by an electron coupling matrix element (V_{star}), resulting in state mixing and the formation of new hybrid states. A major consequence is the "intensity borrowing", where a new low-energy state, mainly the CT-like state, obtaining a small part of the large oscillator strength of the "bright" LE state. This greatly improves the effective oscillator strength of CT to GS transition:

View Article Online
DOI: 10.1039/D5EL00216H

$$f^*_{GS,\,CT} = f_{GS,CT} + \frac{f_{LE,GS}V^2_{star}}{\Delta E^2_{LE,CT}} + \frac{2\sqrt{f_{LE,GS}f_{GS,CT}}V_{star}}{\Delta E_{LE,CT}} \quad (12)$$

This formula shows that the effective oscillator strength increases substantially as the energy offset ($\Delta E_{LE,CT}$) decreases and V_{star} increases. This "brighter" CT state directly increases the radiative recombination rate k_r.

Static energetic disorder is also a key component in this model[50]. The CT state is described by a normalized distribution function for CT-state energies $g(E_{CT})$, which are the sum of multiple weighted gaussian line-shapes $D_t(E_{CT})$, via $g(E_{CT}) = \sum_t c_t D_t(E_{CT})$. For an individual gaussian function, $\sigma_{CT,t}$ is its width and $\langle E_{CT,t}\rangle$ is the energy at its gaussian center:

$$D_t(E_{CT}) = \frac{1}{\sigma_{CT,t}\sqrt{2\pi}} e^{-\frac{\left(E_{CT}-\langle E_{CT,t}\rangle\right)^2}{2\sigma^2_{CT,t}}} \quad (13)$$

The parameter $\sigma_{CT,t}$ quantifies the degree of static disorder for an individual CT manifold t. This is the main cause of the broadening of the low-energy tail in the absorption and emission spectra. Ignoring this distribution will cause the fitting routine to wrongly attribute spectral broadening to artificially exaggerated λ. Because k_{nr} is highly sensitive to λ, it may lead to a significant misjudgment of the recombination rates. Note here that for brevity, we consider single gaussian DOS for later investigations, therefore, subscript "t" is neglected.

We now study the systematic influence of key physical parameters on the accuracy of classical Marcus analysis, including offset between the LE and CT states ($\Delta E_{LE,CT}$), static disorder of CT states (σ_{CT}), coupling between the LE and CT states (V_{star}), low and high frequency reorganization energy of CT state (λ_o and λ_i), CT oscillator strength ($f_{osc.CT}$), and rate constant of LE to CT transition ($k_{LE,CT}$), as shown in **Error! Reference source not found.**. The model parameters used to generate EL and EQE spectra are shown in **Error! Reference source not found.**. By fitting these simulated spectra using the homemade Marcus theory-based program *Marcusfit*[72] (**Error! Reference source not found.**), we can directly compare the fitting parameters (E_{CT} and λ_o) with the known "true" values in the model. $\lambda_{o,model}$ and $E_{CT,model}$ correspond to the low frequency reorganization energy and the free energy of the CT state in the original model, respectively. This analysis reveals several key scenarios where the Classical Marcus analysis fails as shown in **Fig. 4-9** and detailed below.

1) Low offset

We first investigate the case where the LE-CT offset ($\Delta E_{LE,CT}$) is reduced, which is a typical approach to minimize voltage loss experimentally. As shown in **Fig. 4(a-b)**, for large offset systems ($\Delta E_{LE,CT} \geq 0.2$ eV), a distinct CT peak (the bright blue curve

segment) can be observed at the tail of the EQE curve, and E_{CT} and λ_o from Classical Marcus fitting agree reasonably well with the input model values, as shown in **Fig. 4(d)**. On the contrary, for the small offset system (e.g. $\Delta E_{LE,CT} = 0.1$ eV in **Fig. 4(c)**), due to spectral overlap, the EQE tail represents a mixture of the CT and LE absorption, and no clear CT absorption or emission is visible. Since oscillator strength of LE state is usually much larger than that of CT state, the Classical Marcus fit often only captures features of the LE state, leading to overestimated E_{CT} and λ_o due to overlapped emission, as shown in **Fig. 4(d)**. Later, we will show that such result is typical for low offset systems when other properties of CT states change.

2) Large static disorder

We now investigate the case with different static energetic disorders of CT states, i.e. σ_{CT}. As shown in **Fig. 5(a-c)**, for $\Delta E_{LE,CT}$ is fixed at 0.2 eV (moderate offset), the breadth of both EL and EQE get widened with increasing static disorder. The Gaussian line shape of the single-state Marcus model is the result of uniform broadening caused by vibrational electron-phonon coupling. Static disorder, that represents the statistical distribution of molecular site energy due to morphological changes and local electrostatic environment, introduces non-uniform broadening by creating a Gaussian density of states (DOS) for excited states. Therefore, the emission spectrum observed in the experiment is the convolution of the intrinsically uniform line shape with this non-uniform DOS. Under thermal equilibrium, excitons undergo thermal relaxation and migrate to low-energy positions within the DOS before emission. This process causes the emission spectrum to shift to the low energy side, resulting in a wide, asymmetric non-Gaussian distribution in EL, that cannot be easily analyzed by single state Marcus theory. As shown in **Fig. 5(d)**, for systems with low disorder ($\sigma_{CT} < 60$ meV), only E_{CT} values are roughly recovered by Marcus fitting, while λ_o deviates significantly from input values, $\lambda_{o,model}$. For Large static disorder systems, the fitted E_{CT} is systematically severely underestimated due to exciton relaxation in the DOS, in which case, the values of E_{CT} can only be considered as the effective value of CT manifolds[73], rather than the center of CT DOS. In the case of high disorder ($\sigma_{CT} = 120$ meV), the deviation exceeds 0.2 eV. Therefore, λ_o values extracted directly using classical Marcus theory are seriously overestimated. Similar observation is seen with a smaller offset ($\Delta E_{LE,CT}$ = 0.1 eV), as shown in **Error! Reference source not found. (c)**.

3) Strong state hybridization

We now investigate the case with varied electronic coupling (from 0 meV to 80 meV) between the LE and CT states (V_{star}), where the $\Delta E_{LE,CT}$ is fixed at 0.1 eV. When the electronic coupling between LE and CT state rises, there is no longer pure CT or LE state, but rather a combination of both, i.e. a hybrid state. LE states typically exhibit large oscillator strength $f_{LE,GS}$, whereas the oscillator strength of pure CT states (i.e.

View Article Online
DOI: 10.1039/D5EL00216H

$f_{GS,CT}$) is usually several orders of magnitude lower than that of LE[49]. According to **Eq. (15)**, even a small amount of LE component mixed into the CT state leads to a dramatic increase in the effective oscillator strength of the CT state, hence, the change in $f_{GS,CT}$ is the key factor here.

As shown in **Fig. 6(a-c)**, the fitting quality of the classical Marcus theory gradually improves with increasing V_{star}. When V_{star} is small (weak coupling), the CT state cannot acquire sufficient transition dipole moments from the LE state, which renders it intrinsically an optical "dark state". This case is equivalent to the low offset case discussed above, and the Classical Marcus fit only captures the LE state's tail characteristics rather than the true CT state. Consequently, the extracted E_{CT} and λ_o is incorrectly biased toward the higher-energy LE state, as shown in **Fig. 6d**. Conversely, when V_{star} is getting larger (intermediate coupling, e.g. 80 meV), the intensity borrowing effect is activated[49]. The CT state gains substantial oscillator strength, transforming into a "bright state" and forming an independent, distinct absorption peak or shoulder peak, which will lead to slightly better fitting quality, as reflected in **Fig. 6(a-c)**, and reduced fitting errors in **Fig. 6d**. However, it's worth noting here that in all cases when offset is small, noticeably errors appear using the Classical Marcus fit, reflecting results from discussions above. Such behavior is absent in larger offset systems, e.g. 0.2 eV in **Error! Reference source not found. (g)**.

Note here, we are still in the weak to intermediate coupling regime ($V_{star} < 0.5\lambda$)[74], therefore, Fermi's Golden rule and parabolic potential energy surface can still be applied, given the offset between LE and CT state is not smaller than 50 meV[49]. For strong coupling with $V_{star} > 0.5\lambda$ and $\Delta E_{LE,CT} < 50$ meV, parabolic potential energy surface is no longer applicable, and a correction on the wavefunction of CT state is needed, which is beyond the scope of the current work[75].

4) High reorganization energies

We turn to investigate the case with different low and/or high frequency reorganization energy ($\lambda_{o,model}$ and/or $\lambda_{i,model}$) of CT states. For a clearer presentation, we fix the values for $\lambda_{i,model}$, and vary $\lambda_{o,model}$, and finally compare extracted λ_o with input values of $\lambda_{o,model}$, as shown in **Figure 7**. We consider three cases with small (60 meV), medium (90 meV), and large (120 meV) $\lambda_{i,model}$ values for the generation of EL and EQE spectra.

For the spectral fitting, it can be observed that with $\Delta E_{LE,CT}$ = 0.2 eV, a distinct CT peak can be visually identified at the tail of EQE in all cases, as show in **Figure 7**. This provides a reliable reference for extracting E_{CT} and λ_o, leading to good agreements when $\lambda_{o,model}$ is small. However, when $\lambda_{o,model}$ rises, the extracted E_{CT} and λ_o value tends to be inflated. This occurs because as $\lambda_{o,model}$ increases, the CT spectrum widens and extends toward higher energies due to broadening caused by λ_o, significantly increasing the overlap region with the LE state. To fit the blended

View Article Online
DOI: 10.1039/D5EL00216H

spectral edges, the Gaussian function is forced to shift toward higher energies with a widened distribution, leading to an artificially inflated E_{CT} and λ_o, for all cases with different input values of $\lambda_{i,model}$, as shown in **Fig. 7(d,h,l)**. Larger $\lambda_{i,model}$ tends to lead to larger errors due to additional broadening caused by vibronic modes.

In the system with $\Delta E_{LE,CT}$ = 0.3 eV, i.e. larger offset, CT state exhibits spectral characteristics that are well separated from LE state. Therefore, regardless of how the reorganization energy changes in this scenario, classical Marcus theory can accurately extract E_{CT}, as shown in **Error! Reference source not found.(d-f)**. In the MLJ model, the emission exhibits a spectral envelope composed of a series of subpeaks spaced by high-frequency vibrational energy levels ($\hbar\omega$ ≈ 0.15−0.2 eV), where each subpeak's width is determined solely by λ_o and σ_{CT}[50]. When fitting this multi-peak structure using the single Gaussian Marcus theory, the algorithm tends to match the shape of the strongest 0-0 transition main peak. Consequently, the extracted λ_o mainly reflects the $\lambda_{o,model}$ determining the main peak width, while "neglecting" the $\lambda_{i,model}$ that governs the relative intensity of the subpeaks. This explains the good agreement for large offset cases.

In the system with $\Delta E_{LE,CT}$ = 0.1 eV, i.e. small offset, as shown in **Error! Reference source not found.(e-f)**, the extracted E_{CT} is ~0.07 eV larger than the model value. This is due to the strong spectral overlap between LE and CT states, and the classical Marcus fitting effectively fits signal from LE state, yielding an energy value consistently larger than E_{CT} but slightly less than E_{LE}. Thus, the fitted energy at this point actually represents the energy of the mixed LE and CT states. Additionally, the extracted reorganization energy tends to respond weakly to variations in the model reorganization energy. Therefore, the extracted λ_o reflects properties of the mixed LE and CT state, rather than the interfacial CT state. Consequently, regardless of how drastically the model alters the CT state's $\lambda_{o,model}$, as long as these changes do not significantly alter the dominance of the LE state, the values fitted by classical Marcus theory remain "inert". This further demonstrates that in systems with small offset, the direct application of classical Marcus theory is questionable.

5) Low oscillator strength

We now investigate the case with different CT oscillator strength ($f_{osc.CT}$). As shown in **Figure 8(a)**, , for cases with $\Delta E_{LE,CT}$ fixed at 0.2 eV, under low oscillator strength conditions ($f_{osc,CT} = 5 \times 10^{-5}$), the CT state is essentially an optically "dark" state with an extremely low radiative transition rate. Since the intrinsic radiative rate of the LE state is typically several orders of magnitude higher than that of the "dark" CT state, LE emission tends dominate the EL spectrum. Consequently, the observed EL peak is located at the higher-energy LE position rather than the CT position. Therefore, the extracted E_{CT} is erroneously anchored near the LE state's energy, resulting in values significantly higher than the model input CT energy, similar to cases with low offset.

When oscillator strength increases (e.g., $f_{osc.CT} \geq 5 \times 10^{-3}$, **Figure 8(c)**), a clear CT absorption and emission features appear in EQE tail and EL spectrum, respectively. In this case, the Classical Marcus analysis is reasonable, resulting in extracted E_{CT} that align well with model inputs. Interestingly, λ_o extracted by the Classical Marcus theory does not vary with $f_{osc,CT}$ like E_{CT} does, as shown in **Figure 8(d)**. The fitting results remain consistently close to the model reorganization energy values, since we assume identical LE and CT properties apart from their oscillator strength. For a different $\lambda_{o,model}$ value for LE state, changes in λ_o can be expected. The large deviation when $f_{osc,CT} = 5 \times 10^{-3}$ is due to spectral overlapping between LE and CT, leading to broadened emission spectrum. Similar behavior is seen with smaller offset, but not for large offset cases due to good spectral isolation of CT state from LE state, as shown in **Error! Reference source not found.**(a).

Furthermore, we investigate the threshold of I_{CT}/I_{LE}, beyond which the Marcus analysis can be meaningful. As shown in **Error! Reference source not found.**, when I_{CT}/I_{LE} is less than 8 folds, the extracted E_{CT} and λ deviates significantly from the true values. During fitting, it becomes increasingly difficult to obtain good fitting results for the broadening of the CT peak and the intersection of the EL and EQE experimental data curves as I_{CT}/I_{LE} decreases. When the intensity ratio is too small (I_{CT}/I_{LE} < 1), the fitting obtained by forcibly fitting the CT peak is very poor (regardless of how the Marcus fitting parameters are adjusted), while the fitting of the LE peak demonstrates a better visual agreement. Therefore, if the high energy tail of the CT emission is visible with the peak intensity approximately one order of magnitude larger than that from LE states, classical Marcus analysis could lead to meaningful results; otherwise, it should be abandoned.

6) Low charge transfer rate

We last investigate the case with different rate constant of LE to CT transition ($k_{LE,CT}$). When $k_{LE,CT}$ is very large (e.g., 10^{11} s^{-1}), as shown in **Figure 9(a)** for cases where the $\Delta E_{LE,CT}$ is fixed at 0.1 eV, electron transfer is considered to be efficient from LE to CT state, so as the back transfer rate from CT to LE state since CT is populated first in EL experiments. This leads to significant contributions from LE emission to the overall emission spectrum. When this happens, spectral interference from LE again becomes the central problem in the Classical Marcus analysis, hence E_{CT} and λ_o are both overestimated, as also discussed above. At lower rates ($k_{LE,CT} \leq 10^9$ s^{-1}), however the fitted E_{CT} actually approach the model predictions, as shown in **Figure 9(d)**. A lower $k_{LE,CT}$ indicates hindered charge transfer from LE to CT, hence its back transfer from CT to LE. During EL experiments, this means electrical populated CT excitons tend to stay at CT rather than transferring back to LE. At this point, the dominant component of the EL spectrum may shift from LE to CT state emission, leading to much less errors in E_{CT}. The reorganization energy λ_o consistently shows an overestimation, due to the fitting of the mixed CT and LE state emission. Such behavior is, however, not seen

View Article Online
DOI: 10.1039/D5EL00216H

for cases with large offset, i.e. $\Delta E_{LE,CT}$ ≥ 0.2 eV, since CT state will be much more populated than LE state following Boltzmann statistics. Therefore, regardless of $k_{LE,CT}$, as long as CT state luminescence is observed, Marcus fitting can relatively accurately extract parameters, as shown in **Error! Reference source not found.(b)**. This further exemplified the key role of offset in performing the Classical Marcus analysis.

Methods to avoid errors

As discussed above, the invisibility and inherent static disorder of CT states are two of the most important issues for standard single-state Marcus analysis. In particular, the invisible CT state is a common feature in the most efficient OPV based on NFAs. Here we distinguish two cases: 1) visible or partially visible CT states, i.e. the case when CT absorption or emission signal is visible or partially visible and not completely missing; 2) invisible CT states, i.e. the case when CT absorption and emission is completely covered by LE states. We suggest several alternative approaches to measure CT properties when absorption and emission signal is weak from CT states, and provide useful guides to quantitative analysis of CT states.

1. Visible or partially visible CT states

When emission or absorption signal from CT state is not completely covered by LE states, we can still perform the Classical Marcus analysis, but with a modified model considering static disorder. Here we discuss two methods that were proposed in the literature, as follows.

1) Temperature dependent sensitive EQE

The first method is to involve a temperature change during optoelectronic experiment, e.g. temperature-dependent s-EQE as explored by Khan and Rand et al.[52] The benefit of temperature dependent EQE experiment is that the absorption process doesn't involve exciton relaxation in the DOS, hence reducing errors due to unequilibrated excitons that might occur in temperature dependent luminescence experiments. However, such a method requires high resolution of the weak CT absorption band, that should be clearly distinguished from LE absorption band tails.

For the analysis, the experimental EQE spectrum is first measured at different temperatures showing clear features from CT band absorption, followed by fitting using a simple Gaussian function at different temperatures. The extracted apparent E_{CT} $(exp.)$ typically shows a significant downward trend as temperature decreases due to relaxation of excitons in the DOS. At low temperature ($T \rightarrow 0$ K), the line width is limited, which is a temperature-independent feature caused by the static distribution of CT states, i.e. static disorder. The Stokes shift is then no longer fixed at

2λ, which cannot be directly explained by Marcus theory. Burke et al.[73] proposed a physical model that regards the CT state as a Gaussian distribution rather than a single energy level, where the characteristic parameters of the CT state density distribution are the center energy of CT DOS (E_{CT}) and the standard deviation (σ_{CT}) (representing the degree of static disorder). When the Gaussian distribution is convoluted with the dynamic broadening of the molecular vibrations, the resulting absorption spectrum (measured by EQE) can be described by the following expression:

$$\eta_{EQE}(E) \propto \frac{1}{E\sqrt{2\pi\left(\sigma_{CT}^2 + 2\lambda k_B T\right)}} \exp\left(\frac{-(E_{CT} + \lambda - E)^2}{2\sigma_{CT}^2 + 4\lambda k_B T}\right)() \quad (546)$$

Where E is photon energy. This form separates the contribution of static disorder (σ_{CT}^2) and temperature-dependent dynamic disorder ($\sqrt{2\lambda k_B T}$) into total spectral broadening.

It is very important to measure the sub-bandgap region of CT absorption characteristics with high signal-to-noise ratio. Then, the CT absorption features in the EQE spectrum are fitted using the standard Gaussian function at each temperature. The central energy position of the CT feature may be a small peak in the rapid rise phase of the EQE curve. At this time, the apparent experimental parameters peak energy $E_{CT}\,(exp.)$ and apparent recombination energy $\lambda\,(exp.)$at each temperature can be extracted:

$$E_{CT}(exp.) = E_{CT} - \frac{\sigma_{CT}^2}{2k_B T}() \quad (557)$$

$$\lambda(exp.) = \lambda + \frac{\sigma_{CT}^2}{2k_B T}() \quad (558)$$

By plotting the relationship between the extracted $E_{CT}\,(exp.)$ and $\lambda\,(exp.)$ and the reciprocal of temperature ($1/T$), the slopes can be used to extract the true E_{CT} and λ respectively. However, one should be reminded that this method relies on the assumption of Gaussian type DOS, which might not be true in some material systems[76]. A more general type of DOS may be considered to deliver a better resolution of CT properties[50].

2) Spectra deduction (EL-PL)

In the second method, for the system with some but not complete spectral overlap between the LE and CT state emission, an attempt can be made to subtract the appropriately normalized PL spectrum from the EL spectrum to eliminate the LE contribution and leave the residual CT emission signal. As previously explored by Perdigón-Toro et al., assuming that the total EL spectrum is a linear combination of

the CT state emission and the LE state emission, the subtraction of the appropriately normalized PL spectrum from the EL spectrum reveals a broad low-energy residual feature, and the spectrum can theoretically be analyzed in isolation to determine the properties of the CT state[42]. However, such method needs to be carried out with caution, specifically by normalizing the integral area or peak height of the two curves. Since the subtracted signals from EL-PL are often very weak, and may easily be impacted by the levels of injections in EL experiments.

2. Invisible CT states

Invisible CT state refers to the completely covered CT emission and absorption in standard EL and PL experiments. This has now become a common feature and issue in the state-of-the-art NFA based OPVs, making it difficult to acquire properties of CT states, e.g. its state energy and reorganization energies. Here we discuss two methods that have been explored in the literature that can be helpful for probing the invisible CT states.

1) Electro-absorption spectroscopy

The first method is electro-absorption spectroscopy (EAS), also known as Stark spectroscopy[77-80]. EAS is a method to measure the absorbance change (ΔA) caused by the electric field F_{app} by using the external electric field to disturb the molecular ground state and excited state energy level (Stark effect). For a fixed and isotropic sample, the ΔA spectrum can be described by the Liptay equation[81, 82] as a Taylor series expansion:

$$\Delta A = A^F(E) - A(E) = (k-1)A(E) + k\Delta E \cdot \frac{dA}{dE} + \frac{k\Delta E^2}{2} \cdot \frac{d^2A}{dE^2}() \quad (592)$$

Where $A^F(E)$ and $A(E)$ are the absorption spectra with (field-on) and without (field-off) applied field, respectively. The energy change ΔE includes contributions from the linear and quadratic Stark effects:

$$\Delta E = -\frac{1}{2}\Delta p F^2 + () \quad (596)$$

Where Δp and $\Delta\mu$ represent the change in polarizability and dipole moment. And considering the dielectric constant of the medium (ε) in non-polar environments, the effective electric field $F = (2\varepsilon+1)F_{app}/3$ [83].

A Frenkel or local exciton transition refers to the process of electron transition to higher orbitals in the same molecule or chromophore. Its ground state and excited state are relatively non-polar, and the change of $\Delta\mu$ is usually small. Therefore, the EAS signal is mainly affected by the change of polarizability (Δp), and the spectral feature has a linear shape of the first derivative. On the other hand, the CT transition

consists of spatially separated electron-hole pairs ($D^- - A^+$) with a very large electric dipole, and the variation of $\Delta\mu$ is usually larger. Therefore, a strong EAS signal dominated by second-order derivative linear is generated, and the spectral feature is mainly in the form of a second derivative. This means that the shape of the EAS spectrum measured in the experiment is highly similar to the second derivative curve of the absorption peak in the CT state. The central energy of each Gaussian function used to fit the CT absorption band represents the energy of such CT manifold. The fitting formula is:

$$\Delta A \approx \frac{1}{2} C_L \Delta\mu^2 F^2 \frac{d^2 A}{dE^2}()$$

Where the constant C_L is obtained through experiments, with a value of 1/3.

Based on the method described above, the experimental starting point is to obtain absorption spectrum ($A(E)$) in the absence of an applied electric field. Based on this, a known electric field F_{app} is applied to measure the resulting spectral absorption change, namely the electrical absorption spectrum or Stark spectrum (ΔA). After obtaining these two sets of spectral data, the absorption band characteristic attributable to the CT transition must be identified in the $A(E)$ spectrum. To accurately analyze this characteristic and to avoid interference from experimental noise in subsequent calculations, a series of Gaussian functions are typically used to reconstruct or fit the CT absorption band. This step not only provides a spectral line shape that can be accurately differentiated, but also reveals the energy distribution of the CT state attributable to the central energy of the Gaussian functions fitted to the CT absorption band. Finally, to verify the accuracy of such energy distribution, the smoothed absorption spectrum obtained by the Gaussian fitting is first- and second-order differentiated and used as basis functions to fit the experimentally measured ΔA spectrum. This is because the line shape of the electrical absorption signal of the CT state is primarily determined by the second-order derivative of the original absorption spectrum, from which the energy of CT state can be extracted.

2) Advanced model fitting

The final method is to extract CT state properties using the previously developed MLJ model coupled with drift and diffusion equations (which was introduced in the previous section). This theoretical framework allows the modelling of the complete process from exciton generation to charge collection, and the properties of important states, i.e. LE, CT, and charge separated state (CS), are all considered. In a previous study by Muller et al., using this model, they realized simultaneous fitting of current-voltage (JV) characteristics and PL, and extracted CT properties even when it's not visible in EQE, EL and PL[84]. The authors used ΔE_{LE-CT}, LE dissociation rate ($k^{dis}_{LE\rightarrow CT}$), CT dissociation rate ($k^{dis}_{CT\rightarrow CS}$), and mobility ($\mu$) as fitting variables. The absolute PL intensity is used to determine $k^{dis}_{LE\rightarrow CT}$, considering the competition between LE

exciton dissociation and decay[84]. $k_{CT\rightarrow CS}^{dis}$ can be determined from the model by simultaneously fitting J_{sc} and FF. They found $k_{CT\rightarrow CS}^{dis}$ of $10^{10}\ s^{-1}$ for the high-offset blends and of $10^{7}\ s^{-1}$ for the low-offset blends, which are important reasons for low offset systems to deliver low charge generation yield. In addition, by linking the kinetic rate to free energy difference through the principle of detailed balance, the method can extract the energy of charge separated state (E_{CS}) and the energetic barrier between CT and CS, i.e. $\Delta E_{CT,CS}$. This method has the potential to be further explored to include more experimental data in the fitting procedure, to enhance the accuracy of extracted properties of the invisible CT state.

A general guide

Although classical Marcus theory has become a successful and routine tool for analyzing CT states, it requires extra caution when applied to modern high-performance NFA systems. Based on the several advanced methods introduced earlier, we provide the following guide to the probing and analysis of CT states, which is also summered as a decision tree in **Figure 10**.

It is recommended that the first step of any analysis be to carefully examine the low-energy absorption and emission spectra of the device, typically EQE and EL spectra. If the CT features can be clearly seen in the EQE or EL spectra of large offset system either partially or fully, the classic Marcus fitting can be performed. The fitting program *Marcusfit* that we have made public on github will be a very convenient tool[72]. *Marcusfit* is built specifically to streamline this process by jointly analyzing both spectra. It mathematically identifies the intersection point of the normalized EL and EQE curves to establish initial parameter estimates, and employs a fine-tuning algorithm to extract the CT energy and reorganization energy with high numerical stability. However, it is suggested that the obtained CT energy $E_{CT}\ (exp.)$ be interpreted as an effective energy rather than an absolute and single value. This is because the value is affected by the inherent static energetic disorder, causing the experimentally observed emission peak to deviate from the DOS center. Therefore, it is recommended that $E_{CT}\ (exp.)$ be used only as a reference energy. Additionally, the value $\lambda\ (exp.)$ extracted from the classical Marcus fitting contains two physically different phenomena: the dynamic and static disorder. If the extracted reorganization energy (λ_o) from a classical Marcus fit at room temperature is unusually large, static disorder could be significant. The practical strategy is to perform temperature-dependent s-EQE or PL tests. Dynamic disorder is thermally activated and temperature-dependent ($\sigma_d = (2\lambda_o k_B T)^{1/2}$), while static disorder is essentially temperature-independent. Hence, static disorder can be isolated from dynamic effects by measuring the spectra across a range of temperatures and plotting the apparent CT parameters against 1/T.

View Article Online
DOI: 10.1039/D5EL00216H

However, in modern OPVs, LE states are often very emissive, and CT signals are easily buried under that of LE. Hence, the classic Marcus fitting method often fails to yield physically reliable results. When CT absorption is weak, the fitting process usually struggles to capture meaningful CT signals, hence the error would be large. Here, we take the EL and EQE spectra measured by Wu et al.[85] in PM7/IT4F blends as an example and perform classical Marcus fitting, as shown in **Figure 11**. In this case, the small energy difference between the LE and CT states leads to significant overlap between LE and CT emission with peak intensity ratio between CT and LE less than 10, which should give large errors in reorganization energy and CT state energy following the guidance provided in **Figure 10**. Indeed, the fitting parameters extracted from this type of data have significant uncertainties and poor convergence, making it difficult to distinguish the true CT contribution from experimental noise. Therefore, the obtained reorganization energy and CT state energy values lack physical reliability and should be interpreted with caution.

When CT signal is completely obscured by the absorption tail of local excitons. Attempting to fit this region using the classic Marcus model is a common but crucial mistake, as the fitting will mainly focus on the LE tail rather than the CT state, thereby the fitting result is physically meaningless. Therefore, if the CT features cannot be clearly identified via comparing absorption or emission of pristine materials and blends, it is recommended to abandon the classic Marcus fitting. It would be beneficial to consider other methods. For instance, EAS is a powerful technique because it is highly sensitive to changes in the dipole moment (the decisive feature of CT transitions) and can be identified even if the CT state is hidden in conventional absorption spectroscopy[80]. Another approach can also be helpful, that is to employ an advanced model fitting based on MLJ model framework concerning both spectral and device characteristics as explored by Muller et al.[84] Through model fitting multiple experiments, one can obtain the properties of invisible CT states, including but not limited to state energy, inner and outer reorganization energies, static disorder, phonon energies, and the transition rate constants between LE, CT and CS states.

Conclusions

In summary, the classical Marcus single-state theory in the high temperature limit has limitations in the analysis of CT states in modern high-performance NFA based OPVs. The bright local excitonic state emission signal often masks the weak charge transfer state characteristics, and the material itself has static disorder. Therefore, directly applying the Classical Marcus model for fitting may result in values that do not have true significance. We discuss the cause of such issues in detail and provide guidelines to avoid significant errors while doing Marcus analysis of CT states. If CT absorption and emission are visible or partially visible, the extracted values via Marcus fitting

View Article Online
DOI: 10.1039/D5EL00216H

should only be regarded as "effective energies" given the static disorder is present. Meanwhile, the reorganization energies obtained through Marcus fitting should be treated with caution. It's suggested to employ temperature dependent spectroscopy to better resolve the impact of dynamic and static disorder. If the characteristics of the charge transfer state cannot be clearly identified in the sub-bandgap regions of the absorption and emission spectra, the classic Marcus fitting should be abandoned and advanced techniques such as electro-absorption spectroscopy should be adopted instead. Advanced models concerning more practical features of CT states can also be useful and can help extract more information about the hidden CT states.

View Article Online
DOI: 10.1039/D5EL00216H

Data availability

All the data supporting the current study are available in its Supplementary Material files or from the corresponding authors upon reasonable request. The code is available via GitHub: https://github.com/junyannj/Marcusfit.

Acknowledgements

J.Y. acknowledges funding support from National Natural Science Foundation of China (No. 62574175 and No. 62404191), Guangdong Basic and Applied Basic Research Foundation (No. 2023A1515111140 and No. 2024A1515012318), Guangdong Provincial Program (No. 2023QN10C144), Shenzhen Science and Technology Program (No. KQTD20240729102028011 and No. JCYJ20240813113553067), and Guangdong Basic Research Center of Excellence for Aggregate Science.

Author contributions

L.L. and J.Y. wrote the manuscript. L.L. conducted model calculations and developed *Marcusfit*. S.L., W.L., and X.L. gave critical review of the manuscript. J.Y. supervised the work.

Competing interests

The authors declare no competing interests.

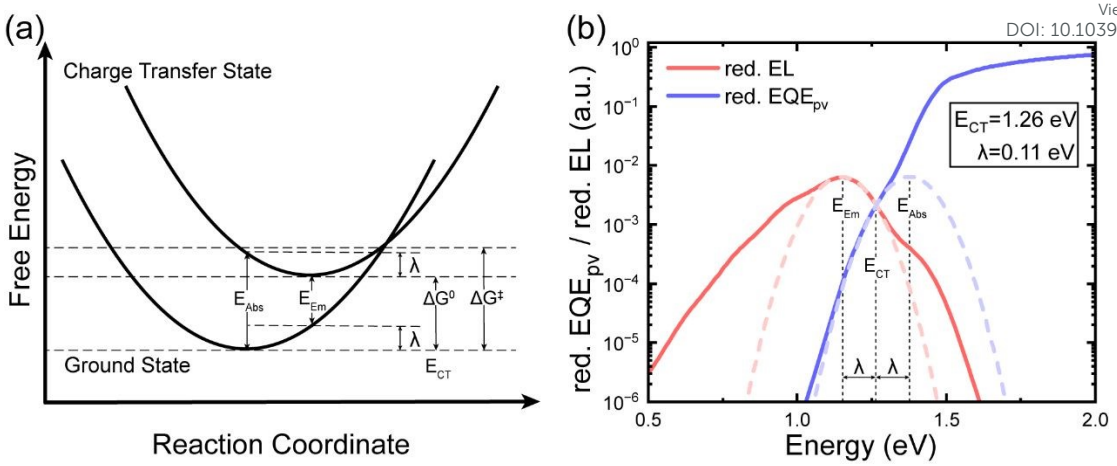

747

748 **Fig. 1** (a) Schematic diagram of the evolution of potential energies for the ground state and
749 charge transfer state along the reaction coordinate, for harmonic potentials. ΔG^0 represents
750 the Gibbs free energy change of the reaction, and $\Delta G^{\ddagger}$ represents the activation barrier; (b)
751 Schematic diagram of Marcus theory fit of the reduced EQE_{PV} and EL spectra. In (a) and (b),
752 E_{abs} and E_{em} represent the energies of maximum absorption and emission, respectively;
753 E_{CT} represents to the charge transfer state energy, and λ represents the reorganization
754 energy.

755

View Article Online
DOI: 10.1039/D5EL00216H

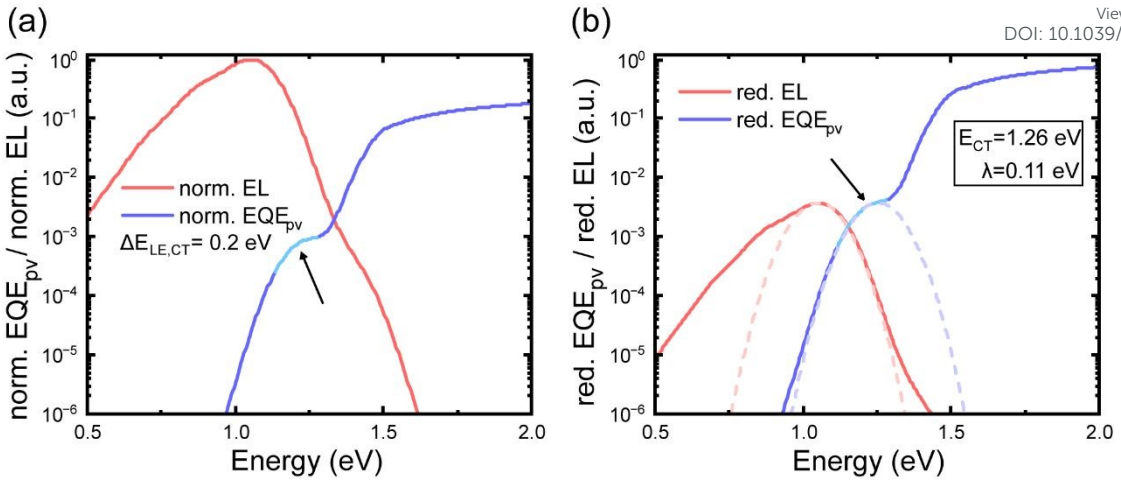

Fig. 2 Schematic diagram of the steps involved in fitting EL and EQE spectra using Marcus theory. (a) The first step is to normalize the experimental EL and EQE data. A clear CT absorption peak (the bright blue curve segment) is observed in the normalized EQE_{PV} (norm. EQE_{PV}) curve. (b) The second step is to shift the main peak of the reduced electroluminescence ($red.EL$) spectrum downward so that its intensity matches with the CT peak in the reduced EQE_{PV} ($red.EQE_{PV}$) spectrum. The dashed Gaussian line represents the fitting result based on Classical Marcus theory.

View Article Online
DOI: 10.1039/D5EL00216H

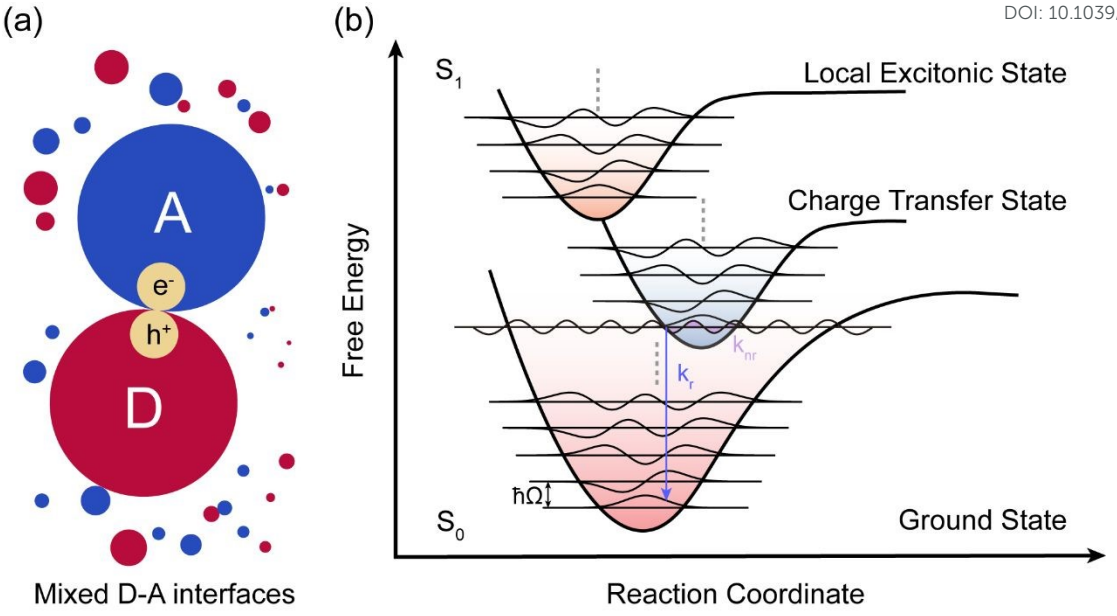

765

766 **Fig. 3** (a) Schematic diagram of an electron and hole occupying the interfacial CT states at the
767 junction of the donor domain (red) and the acceptor domain (blue); (b) The potential energy
768 surface plot depicts the evolution of potential energies for the ground state, charge transfer
769 state, and local excitonic state along the reaction coordinate. The ground state is shown in
770 red, the local excitonic state in orange, and the charge transfer state in blue. Blue arrows
771 indicate radiative decay pathways, while the pink shaded area (indicating the overlap between
772 the vibrational modes of the lowest CT state and those of the highest ground state) represent
773 non-radiative recombination pathways.

774

View Article Online
DOI: 10.1039/D5EL00216H

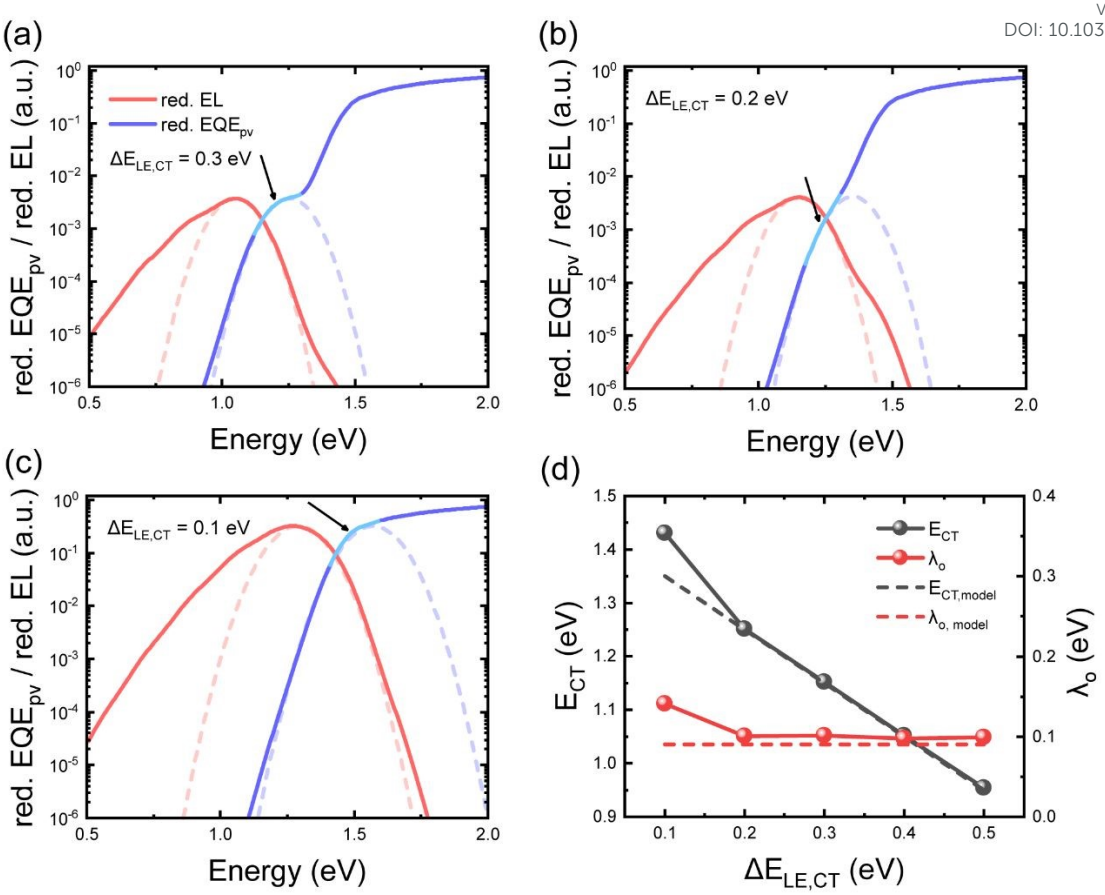

Fig. 4 Summary of the results for different offsets ($\Delta E_{LE,CT}$) via fitting EL and EQE spectra using the Classical Marcus theory. When performing Marcus fitting on the results with offsets of (a) 0.3 eV, (b) 0.2 eV, and (c) 0.1 eV, the bright blue curve segment is a reference marker indicating the downward shift of the main peak of the $red.EL$ spectrum. (d) Comparison between the physical parameters of the original model and the Classical Marcus fit results. The previously developed model[49, 50, 69, 71] was used to generate EL and EQE data, with input parameters as shown in **Error! Reference source not found.**. The dotted line represents the parameters set in the original model, and the solid line represents the result obtained by the Classical Marcus fitting. $\lambda_{o,model}$ corresponds to the low frequency reorganization energy of the CT state in the original model, and $E_{CT,model}$ corresponds to the free energy of the CT state.

View Article Online
DOI: 10.1039/D5EL00216H

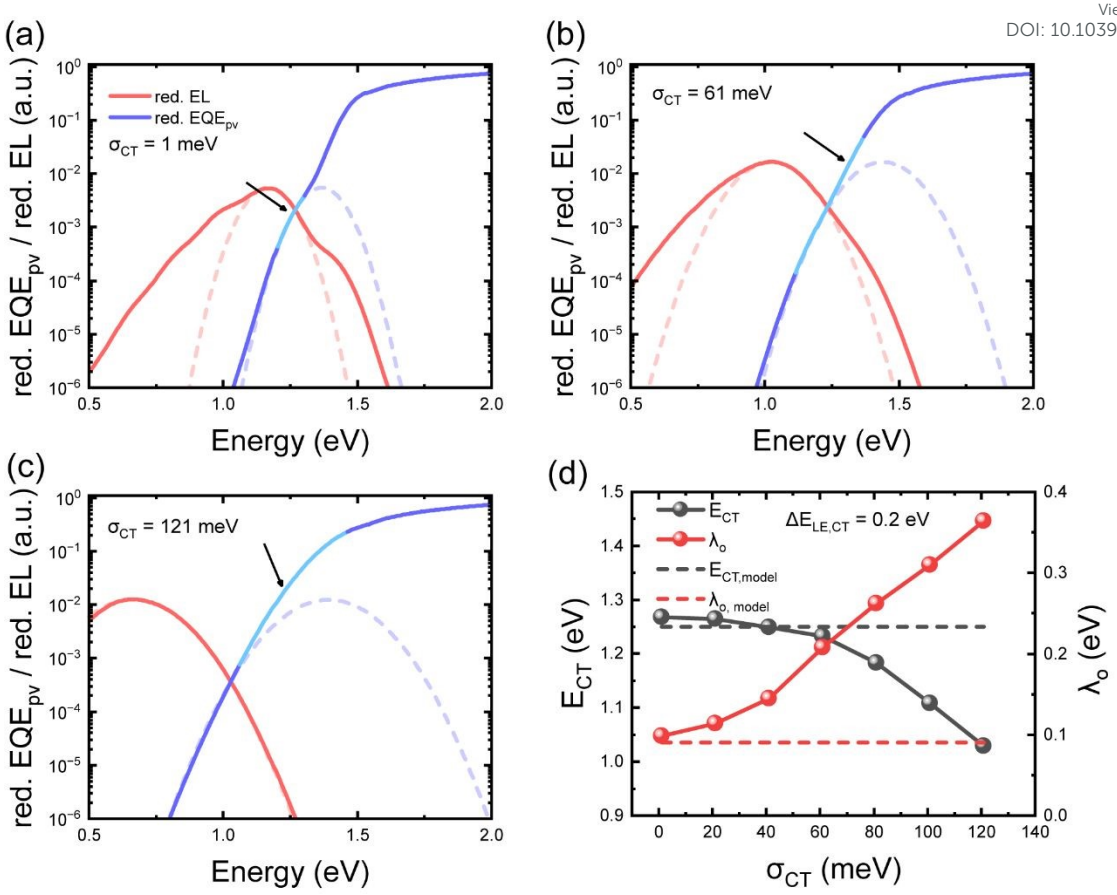

788

789 **Fig. 5 Summary of the results for different static disorder (σ_{CT}) with $\Delta E_{LE,CT}$ = 0.2 eV via**
790 **fitting EL and EQE spectra using the Classical Marcus theory.** When performing Marcus fitting
791 on the results with static disorder of (a) 1 meV, (b) 61 meV, and (c) 121 meV, the bright blue
792 curve segment is a reference marker indicating the downward shift of the main peak of the
793 $red.EL$ spectrum. (d) Comparison between the physical parameters of the original model and
794 the Classical Marcus fit results. The previously developed model was used to generate EL and
795 EQE data, with input parameters as shown in **Error! Reference source not found.**. The dotted
796 line represents the parameters set in the original model, and the solid line represents the
797 result obtained by the Classical Marcus fitting. $\lambda_{o,model}$ corresponds to the low frequency
798 reorganization energy of the CT state in the original model, and $E_{CT,model}$ corresponds to
799 the free energy of the CT state.

800

801

802

View Article Online
DOI: 10.1039/D5EL00216H

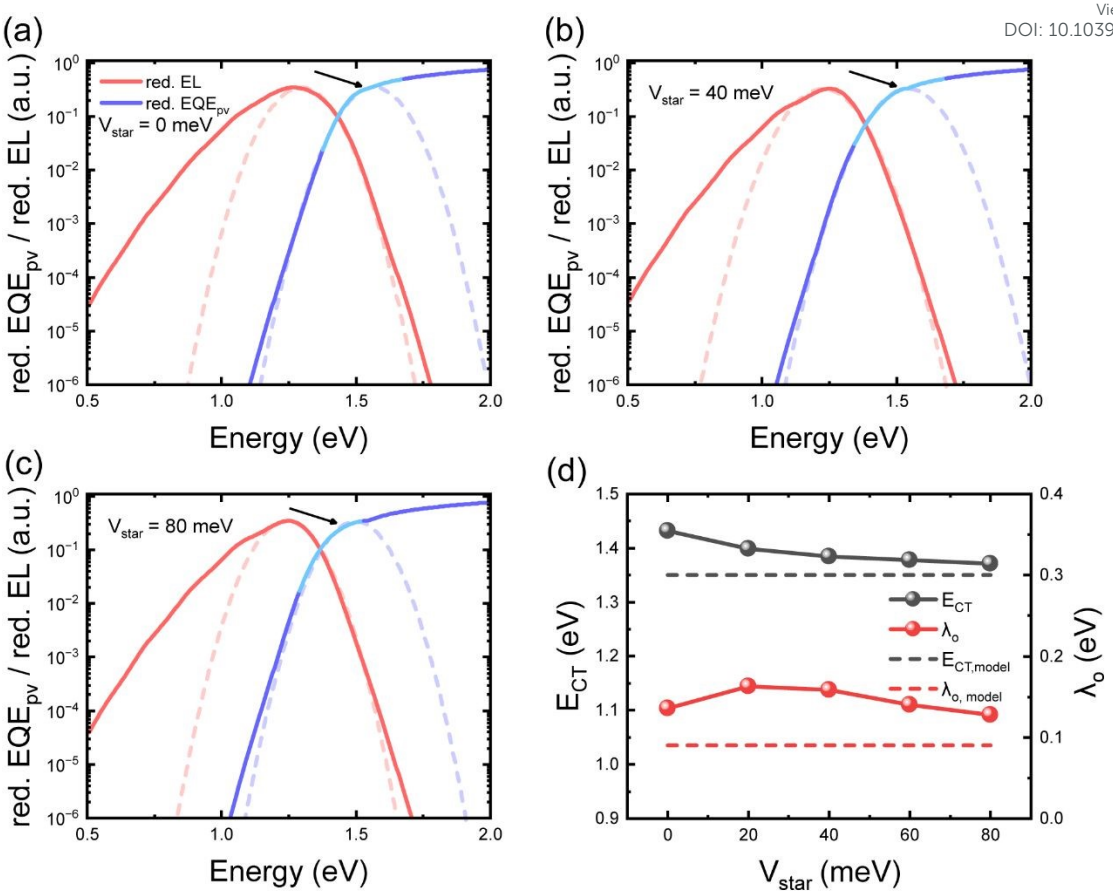

Fig. 6 Summary of the results for different state hybridization (V_{star}) with $\Delta E_{LE,CT}$ = 0.1 eV via fitting EL and EQE spectra using the Classical Marcus theory. When performing Marcus fitting on the results with state hybridization of (a) 0 meV, (b) 40 meV, and (c) 80 meV, the bright blue curve segment is a reference marker indicating the downward shift of the main peak of the $red.EL$ spectrum. (d) Comparison between the physical parameters of the original model and the Classical Marcus fit results. The previously developed model was used to generate EL and EQE data, with input parameters as shown in **Error! Reference source not found.**. The dotted line represents the parameters set in the original model, and the solid line represents the result obtained by the Classical Marcus fitting. $\lambda_{o,model}$ corresponds to the low frequency reorganization energy of the CT state in the original model, and $E_{CT,model}$ corresponds to the free energy of the CT state.

View Article Online
DOI: 10.1039/D5EL00216H

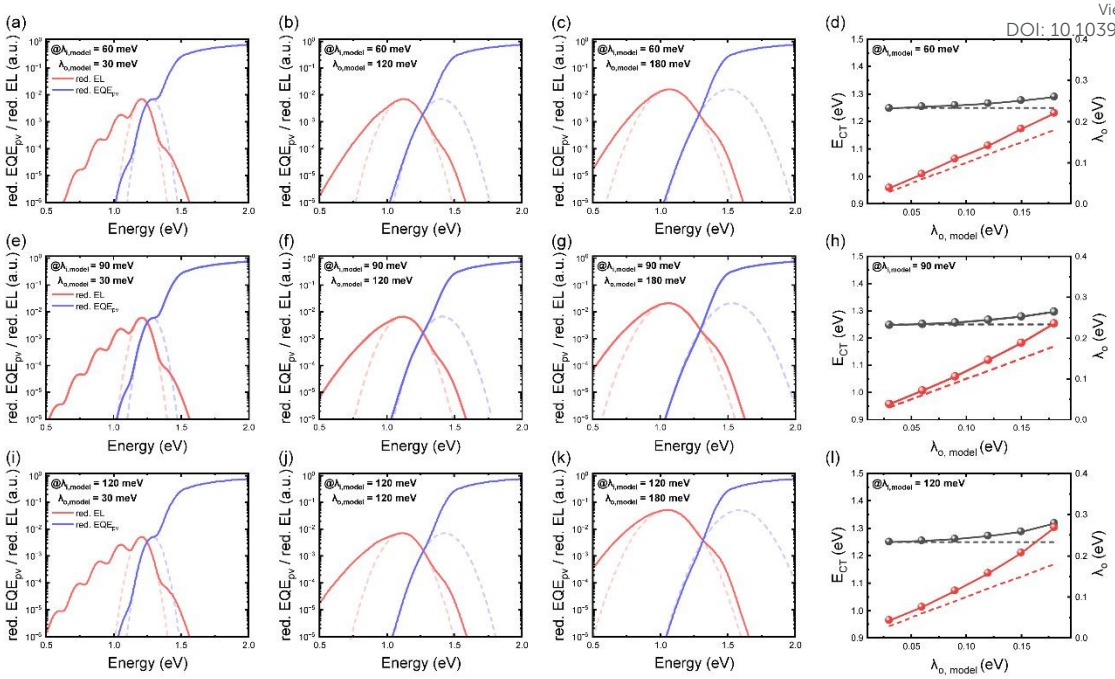

817

818 **Figure 7 Summary of the results for different CT low and/or high frequency reorganization**
819 **energy (λ_o and/or λ_i) with $\Delta E_{LE,CT}$ = 0.2 eV via fitting EL and EQE spectra using the**
820 **Classical Marcus theory.** Input values ($\lambda_{i,model}$ and $\lambda_{o,model}$) for the model for generating EL
821 and EQE spectral data are fixed as (a-d)$\lambda_{i,model}$ = 60 meV; (e-h)$\lambda_{i,model}$ = 90 meV; (i-l)
822 $\lambda_{i,model}$ = 120 meV with different $\lambda_{o,model}$. (d), (h), and (l) Comparison between the physical
823 parameters of the original model and the Classical Marcus fit results. The previously
824 developed model was used to generate EL and EQE data, with input parameters as shown in
825 **Error! Reference source not found.**. The dotted line represents the parameters set in the
826 original model, and the solid line represents the result obtained by the Classical Marcus fitting.
827 $\lambda_{o,model}$ corresponds to the low frequency reorganization energy of the CT state in the
828 original model, and $E_{CT,model}$ corresponds to the free energy of the CT state.

829

830

View Article Online
DOI: 10.1039/D5EL00216H

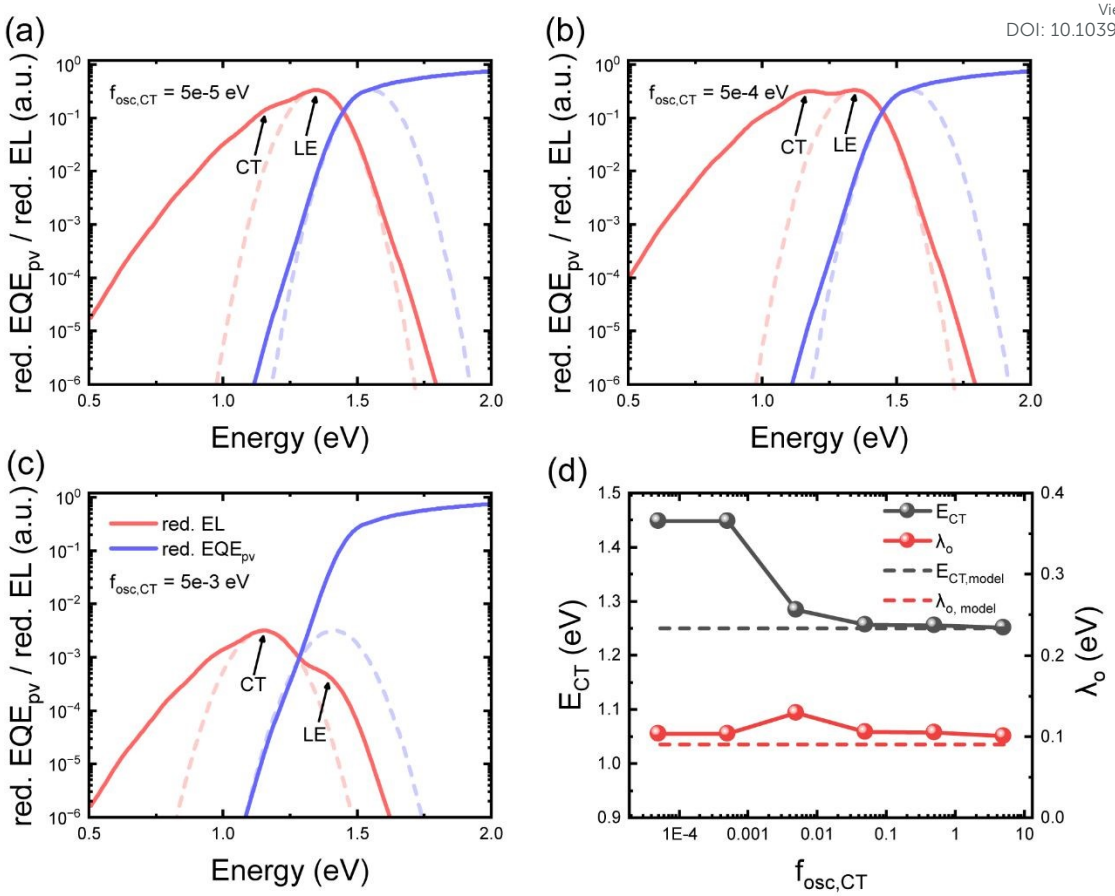

Figure 8 Summary of the results for different CT oscillator strength ($f_{osc.CT}$) with $\Delta E_{LE,CT}$ = 0.2 eV via fitting EL and EQE spectra using the Classical Marcus theory. (a-c) Fits obtained using an $f_{osc.CT}$ of 5×10^{-5}, 5×10^{-4}, and 5×10^{-3}, respectively. (d) Comparison between the physical parameters of the original model and the Classical Marcus fit results. The previously developed model was used to generate EL and EQE data, with input parameters as shown in **Error! Reference source not found.**. The dotted line represents the parameters set in the original model, and the solid line represents the result obtained by the Classical Marcus fitting. $\lambda_{o,model}$ corresponds to the low frequency reorganization energy of the CT state in the original model, and $E_{CT,model}$ corresponds to the free energy of the CT state.

View Article Online
DOI: 10.1039/D5EL00216H

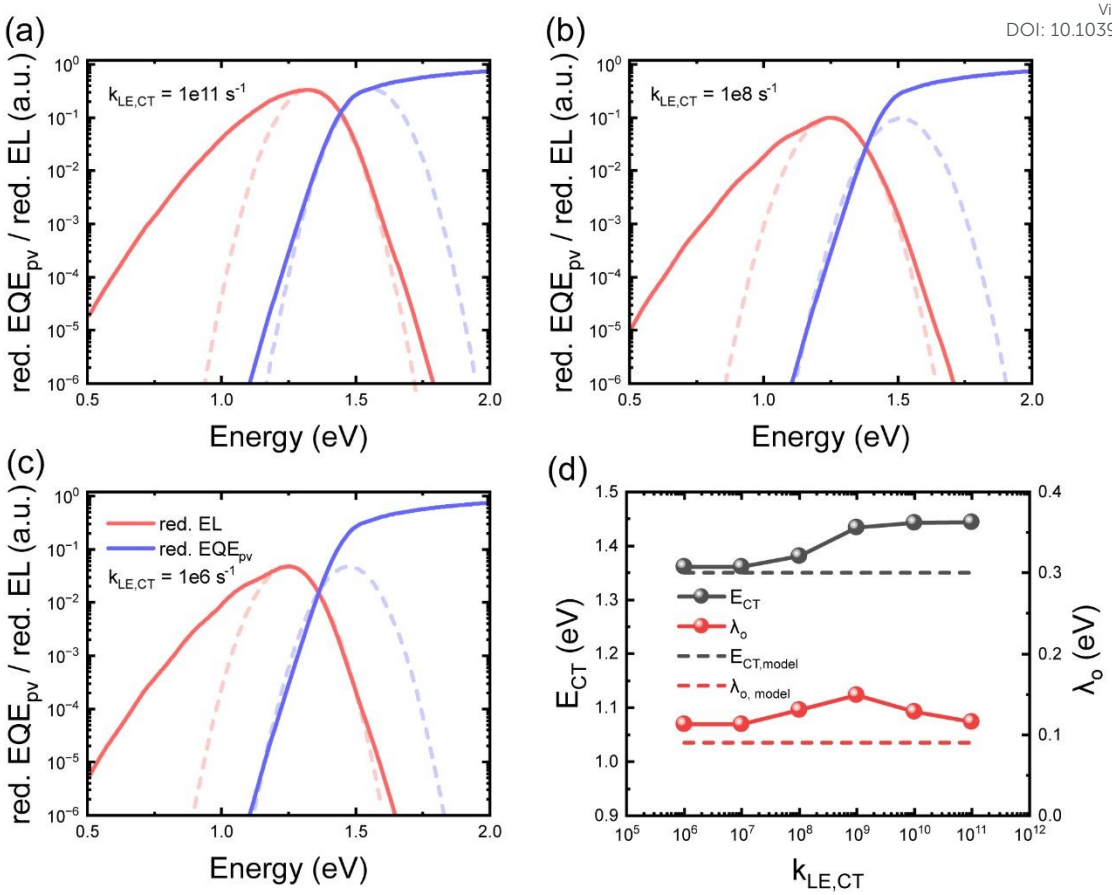

Figure 9 Summary of the results for different rate constant of LE to CT states ($k_{LE,CT}$) with $\Delta E_{LE,CT}$ = 0.1 eV via fitting EL and EQE spectra using the Classical Marcus theory. (a-c) Fits obtained using an $k_{LE,CT}$ of 10^{11}, 10^{9}, and 10^{6} s^{-1}, respectively. (d) Comparison between the physical parameters of the original model and the Classical Marcus fit results. The previously developed model was used to generate EL and EQE data, with input parameters as shown in **Error! Reference source not found.**. The dotted line represents the parameters set in the original model, and the solid line represents the result obtained by the Classical Marcus fitting. $\lambda_{o,model}$ corresponds to the low frequency reorganization energy of the CT state in the original model, and $E_{CT,model}$ corresponds to the free energy of the CT state.

View Article Online
DOI: 10.1039/D5EL00216H

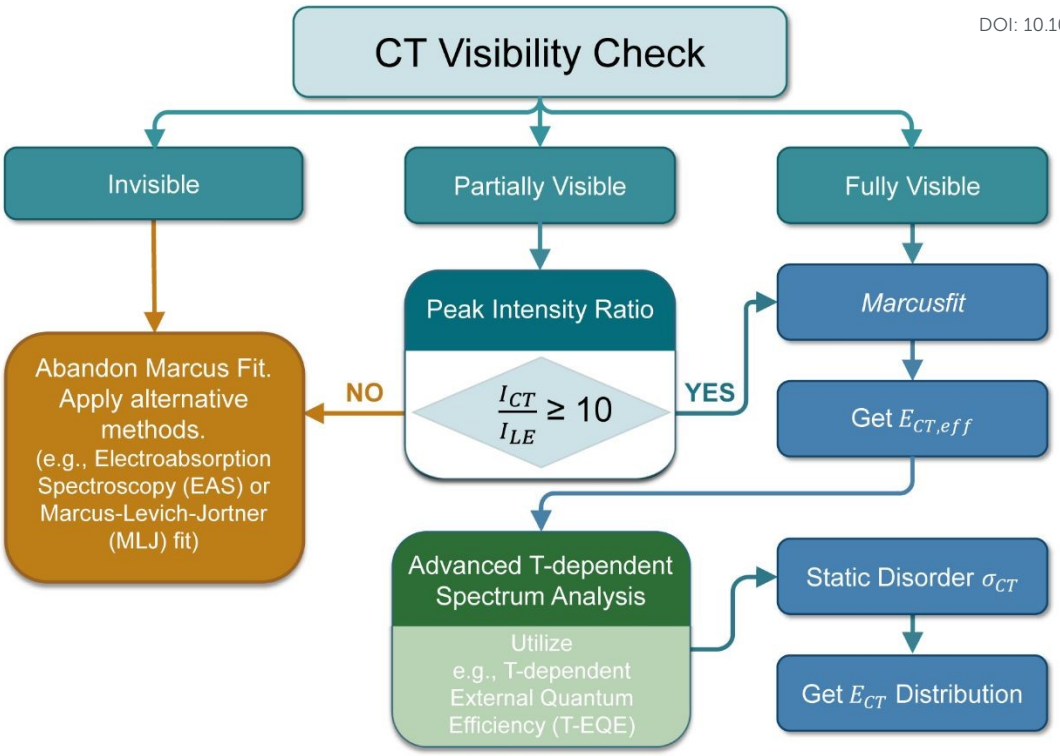

856

857 **Figure 10 Decision tree for Marcus fitting of EQE_{PV} and EL spectra.** The flowchart outlines a
858 systematic protocol based on the visibility of CT emission feature in EL experimental spectra.
859 Starting with a "CT Visibility Check," the procedure branches into three pathways: (i) Invisible.
860 Marcus fitting is abandoned in favor of alternative methods such as Electroabsorption
861 Spectroscopy (EAS) or Marcus-Levich-Jortner (MLJ) fitting; (ii) Partially Visible. The peak
862 intensity ratio $\boldsymbol{I_{CT}/I_{LE}}$ is evaluated; if ≥10, Marcus fitting proceeds to obtain effective CT
863 energy ($\boldsymbol{E_{CT,eff}}$), followed by advanced temperature-dependent spectral analysis (e.g., T-EQE)
864 to extract static disorder ($\boldsymbol{\sigma_{CT}}$) and the final $\boldsymbol{E_{CT}}$ distribution; otherwise, alternative methods
865 are applied; (iii) Fully Visible. Marcus fitting is directly applied to derive $\boldsymbol{E_{CT,eff}}$, then refined
866 via temperature-dependent analysis to yield $\boldsymbol{\sigma_{CT}}$ and the final $\boldsymbol{E_{CT}}$ distribution.

867

868

View Article Online
DOI: 10.1039/D5EL00216H

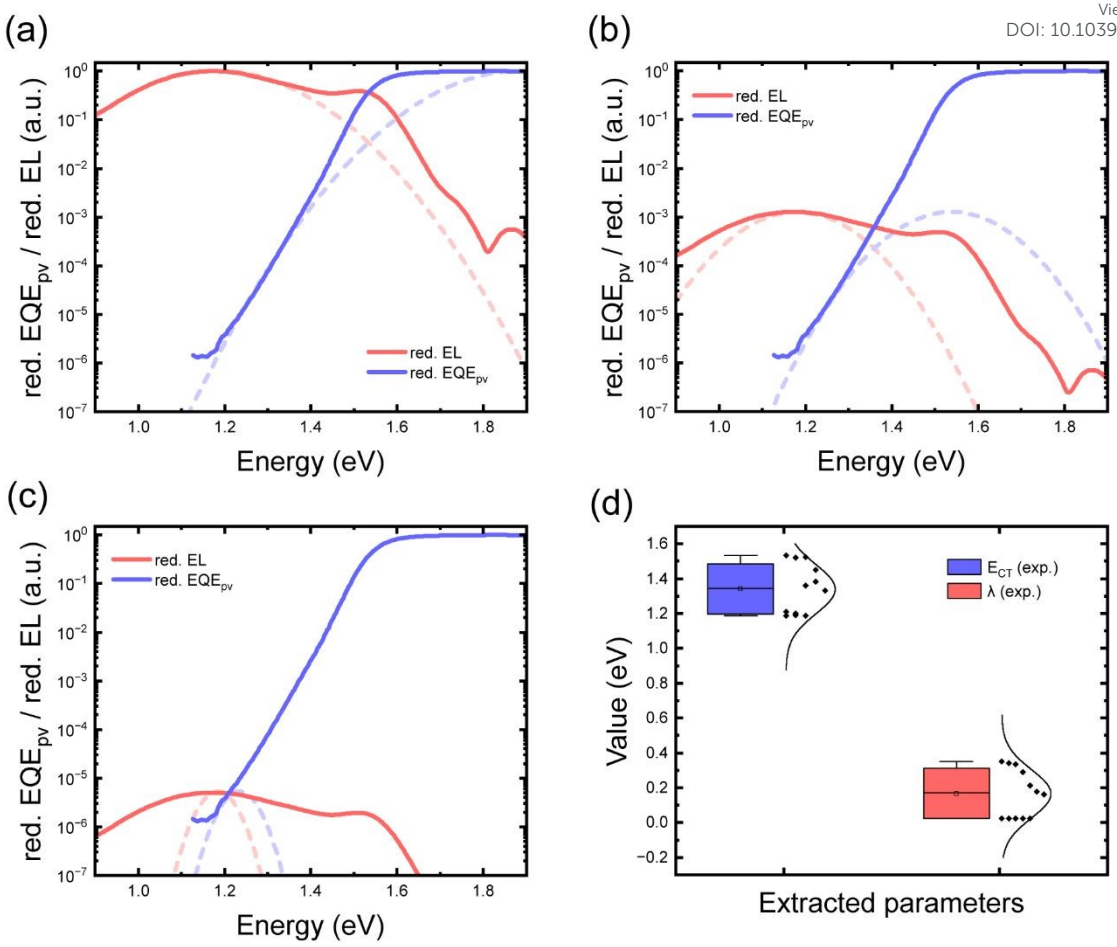

Figure 11 Summary of the results for fitting EL and EQE spectra of PM7/IT4F blends[85] using the Classical Marcus theory. (a-c) The fitting results for either the shoulder peak or the EQE tail are difficult to simultaneously fit spectral features such as peak intensity, linewidth, and the intersection of the EL and EQE curves. (d) Error statistics of results from multiple fittings using the classic Marcus fitting.

View Article Online
DOI: 10.1039/D5EL00216H

References

1. N. S. Hush and J. R. Reimers, *Coordination Chemistry Reviews*, 1998, **177**, 37-60.
2. M. Bixon and J. Jortner, in *Advances in Chemical Physics*, 1999, pp. 35-202.
3. N. Sutin, in *Advances in Chemical Physics*, 1999, pp. 7-33.
4. K. C. Weston, *Energy Conversion*, West Publishing Company, 1992.
5. P. Würfel, *Physics of Solar Cells: From Principles to New Concepts*, Wiley-VCH Verlag GmbH, Weinheim., 2005.
6. S. R. Wenham, *Applied Photovoltaics*, Earthscan, 2007.
7. J. Nelson, *The Physics of Solar Cells*, World Scientific Publishing Company, 2003.
8. R. A. Marcus, *Reviews of Modern Physics*, 1993, **65**, 599-610.
9. R. A. Marcus, *Discussions of the Faraday Society*, 1960, **29**, 21-31.
10. R. A. Marcus, *The Journal of Chemical Physics*, 1956, **24**, 966-978.
11. W. F. Libby, *The Journal of Physical Chemistry*, 1952, **56**, 863-868.
12. R. A. Marcus, *Faraday Discussions of the Chemical Society*, 1982, **74**, 7-15.
13. R. A. Marcus, *Annual Review of Physical Chemistry*, 1964, **15**, 155-196.
14. R. A. Marcus, *The Journal of Physical Chemistry*, 1963, **67**, 853-857.
15. E. V. Anslyn and D. A. Dougherty, *Modern Physical Organic Chemistry*, University Science Books, 2006.
16. R. A. Marcus, *The Journal of Physical Chemistry*, 1968, **72**, 891-899.
17. J. Stubbe, D. G. Nocera, C. S. Yee and M. C. Chang, *Chem Rev*, 2003, **103**, 2167-2201.
18. J. Franck and E. G. Dymond, *Transactions of the Faraday Society*, 1926, **21**, 536-542.
19. E. Condon, *Physical Review*, 1926, **28**, 1182-1201.
20. J. R. Miller, L. Calcaterra and G. Closs, *Journal of the American Chemical Society*, 1984, **106**, 3047-3049.
21. G. L. Closs and J. R. Miller, *Science*, 1988, **240**, 440-447.
22. J. Benduhn, K. Tvingstedt, F. Piersimoni, S. Ullbrich, Y. Fan, M. Tropiano, K. A. McGarry, O. Zeika, M. K. Riede, C. J. Douglas, S. Barlow, S. R. Marder, D. Neher, D. Spoltore and K. Vandewal, *Nature Energy*, 2017, **2**, 17053.
23. E. Collado-Fregoso, S. N. Pugliese, M. Wojcik, J. Benduhn, E. Bar-Or, L. Perdigón Toro, U. Hörmann, D. Spoltore, K. Vandewal, J. M. Hodgkiss and D. Neher, *Journal of the American Chemical Society*, 2019, **141**, 2329-2341.
24. P. F. Barbara, T. J. Meyer and M. A. Ratner, *The Journal of Physical*

View Article Online
DOI: 10.1039/D5EL00216H

Chemistry, 1996, **100**, 13148-13168.
25. G. Pourtois, D. Beljonne, J. Cornil, M. A. Ratner and J. L. Brédas, *Journal of the American Chemical Society*, 2002, **124**, 4436-4447.
26. Y.-A. Duan, Y. Geng, H.-B. Li, J.-L. Jin, Y. Wu and Z.-M. Su, *Journal of Computational Chemistry*, 2013, **34**, 1611-1619.
27. L. Liu, P. Eisenbrandt, T. Roland, M. Polkehn, P.-O. Schwartz, K. Bruchlos, B. Omiecienski, S. Ludwigs, N. Leclerc, E. Zaborova, J. Léonard, S. Méry, I. Burghardt and S. Haacke, *Physical Chemistry Chemical Physics*, 2016, **18**, 18536-18548.
28. M. List, T. Sarkar, P. Perkhun, J. Ackermann, C. Luo and U. Würfel, *Nature Communications*, 2018, **9**, 3631.
29. J. Wang, H. Yao, Y. Xu, L. Ma and J. Hou, *Materials Chemistry Frontiers*, 2021, **5**, 709-722.
30. K. Vandewal, K. Tvingstedt, A. Gadisa, O. Inganäs and J. V. Manca, *Physical Review B*, 2010, **81**, 125204.
31. J. Benduhn, F. Piersimoni, G. Londi, A. Kirch, J. Widmer, C. Koerner, D. Beljonne, D. Neher, D. Spoltore and K. Vandewal, *Advanced Energy Materials*, 2018, **8**, 1800451.
32. V. Coropceanu, X.-K. Chen, T. Wang, Z. Zheng and J.-L. Brédas, *Nature Reviews Materials*, 2019, **4**, 689-707.
33. A. A. Bakulin, S. D. Dimitrov, A. Rao, P. C. Y. Chow, C. B. Nielsen, B. C. Schroeder, I. McCulloch, H. J. Bakker, J. R. Durrant and R. H. Friend, *The Journal of Physical Chemistry Letters*, 2013, **4**, 209-215.
34. J. Hustings, R. Bonné, R. Cornelissen, F. Morini, R. Valcke, K. Vandewal and J. V. Manca, *Frontiers in Photonics*, 2022, **3**.
35. K. Vandewal, J. Benduhn and V. C. Nikolis, *Sustainable Energy & Fuels*, 2018, **2**, 538-544.
36. Y. Jiang, S. Sun, R. Xu, F. Liu, X. Miao, G. Ran, K. Liu, Y. Yi, W. Zhang and X. Zhu, *Nature Energy*, 2024, **9**, 975-986.
37. J. Fu, H. Li, H. Liu, P. Huang, H. Chen, P. W. K. Fong, T. A. Dela Peña, M. Li, X. Lu, P. Cheng, Z. Xiao, S. Lu and G. Li, *Nature Energy*, 2025, **10**, 1251-1261.
38. H. Chen, Y. Huang, R. Zhang, H. Mou, J. Ding, J. Zhou, Z. Wang, H. Li, W. Chen, J. Zhu, Q. Cheng, H. Gu, X. Wu, T. Zhang, Y. Wang, H. Zhu, Z. Xie, F. Gao, Y. Li and Y. Li, *Nature Materials*, 2025, **24**, 444-453.
39. C. Li, J. Song, H. Lai, H. Zhang, R. Zhou, J. Xu, H. Huang, L. Liu, J. Gao, Y. Li, M. H. Jee, Z. Zheng, S. Liu, J. Yan, X.-K. Chen, Z. Tang, C. Zhang, H. Y. Woo, F. He, F. Gao, H. Yan and Y. Sun, *Nature Materials*, 2025, **24**, 433-443.
40. Y. Shi, Y. Chang, K. Lu, Z. Chen, J. Zhang, Y. Yan, D. Qiu, Y. Liu, M. A. Adil, W. Ma, X. Hao, L. Zhu and Z. Wei, *Nature Communications*, 2022,

View Article Online
DOI: 10.1039/D5EL00216H

13, 3256.

41. P. Cheng, G. Li, X. Zhan and Y. Yang, *Nature Photonics*, 2018, **12**, 131-142.
42. L. Perdigón-Toro, L. Q. Phuong, S. Zeiske, K. Vandewal, A. Armin, S. Shoaee and D. Neher, *ACS Energy Letters*, 2021, **6**, 557-564.
43. N. A. Ran, S. Roland, J. A. Love, V. Savikhin, C. J. Takacs, Y. T. Fu, H. Li, V. Coropceanu, X. Liu, J. L. Brédas, G. C. Bazan, M. F. Toney, D. Neher and T. Q. Nguyen, *Nat Commun*, 2017, **8**, 79.
44. D. Qian, S. M. Pratik, Q. Liu, Y. Dong, R. Zhang, J. Yu, N. Gasparini, J. Wu, T. Zhang, V. Coropceanu, X. Guo, M. Zhang, J.-L. Bredas, F. Gao and J. R. Durrant, *Advanced Energy Materials*, 2023, **13**, 2301026.
45. F. Gao and O. Inganäs, *Physical Chemistry Chemical Physics*, 2014, **16**, 20291-20304.
46. S. Few, J. M. Frost and J. Nelson, *Physical Chemistry Chemical Physics*, 2015, **17**, 2311-2325.
47. Y. Zhong, M. Causa', G. J. Moore, P. J. Krauspe, B. Xiao, F. Günther, J. Kublitski, R. Shivhare, J. Benduhn, E. Baror, S. Mukherjee, K. M. Yallum, J. Réhault, S. C. B. Mannsfeld, D. Neher, L. J. Richter, D. M. Delongchamp, F. Ortmann, K. Vandewal, E. Zhou and N. Banerji, *Nature Communications*, 2020, **11**.
48. X.-K. Chen, V. Coropceanu and J.-L. Brédas, *Nature Communications*, 2018, **9**, 5295.
49. F. D. Eisner, M. Azzouzi, Z. Fei, X. Hou, T. D. Anthopoulos, T. J. S. Dennis, M. Heeney and J. Nelson, *Journal of the American Chemical Society*, 2019, **141**, 6362-6374.
50. J. Yan, E. Rezasoltani, M. Azzouzi, F. Eisner and J. Nelson, *Nature Communications*, 2021, **12**, 3642.
51. C. Kaiser, O. J. Sandberg, N. Zarrabi, W. Li, P. Meredith and A. Armin, *Nature Communications*, 2021, **12**, 3988.
52. S.-U.-Z. Khan and B. P. Rand, *Physical Review Applied*, 2021, **16**, 044026.
53. S. M. Hosseini, S. Wilken, B. Sun, F. Huang, S. Y. Jeong, H. Y. Woo, V. Coropceanu and S. Shoaee, *Advanced Energy Materials*, 2023, **13**.
54. C. Göhler, M. Saladina, Y. Wang, D. Spoltore, J. Benduhn, K. Leo and C. Deibel, 2021.
55. F.-J. Kahle, A. Rudnick, S. Wedler, R. Saxena, R. Ammenhäuser, U. Scherf, S. Bagnich, H. Bässler and A. Köhler, *Advanced Energy Materials*, 2022, **12**, 2103063.
56. R. A. Marcus and N. Sutin, *Biochimica et Biophysica Acta (BBA) - Reviews on Bioenergetics*, 1985, **811**, 265-322.
57. Y. Georgievskii, C.-P. Hsu and R. Marcus, *The Journal of chemical*

View Article Online
DOI: 10.1039/D5EL00216H

physics, 1999, **110**, 5307-5317.
58. J. Jortner, *The Journal of Chemical Physics*, 1976, **64**, 4860-4867.
59. J. Nelson, J. J. Kwiatkowski, J. Kirkpatrick and J. M. Frost, *Accounts of Chemical Research*, 2009, **42**, 1768-1778.
60. A. Migliore and A. Nitzan, *ACS Nano*, 2011, **5**, 6669-6685.
61. Y. Zhao and W. Liang, *Chemical Society Reviews*, 2012, **41**, 1075-1087.
62. A. Köhler and H. Bässler, *Electronic processes in organic semiconductors: An introduction*, John Wiley & Sons, 2015.
63. E. Kennard, *Physical Review*, 1918, **11**, 29.
64. P. Moroshkin, L. Weller, A. Saß, J. Klaers and M. Weitz, *Physical Review Letters*, 2014, **113**, 063002.
65. U. Rau, *Physical Review B*, 2007, **76**, 085303.
66. W. Shockley, *Bell system technical journal*, 1949, **28**, 435-489.
67. K. Vandewal, K. Tvingstedt and O. Inganäs, in *Semiconductors and Semimetals*, eds. U. Wüerfel, M. Thorwart and E. R. Weber, Elsevier, 2011, vol. 85, pp. 261-295.
68. K. Vandewal, A. Gadisa, W. D. Oosterbaan, S. Bertho, F. Banishoeib, I. Van Severen, L. Lutsen, T. J. Cleij, D. Vanderzande and J. V. Manca, *Advanced Functional Materials*, 2008, **18**, 2064-2070.
69. M. Azzouzi, J. Yan, T. Kirchartz, K. Liu, J. Wang, H. Wu and J. Nelson, *Physical Review X*, 2018, **8**, 031055.
70. A. Classen, C. L. Chochos, L. Lüer, V. G. Gregoriou, J. Wortmann, A. Osvet, K. Forberich, I. McCulloch, T. Heumüller and C. J. Brabec, *Nature Energy*, 2020, **5**, 711-719.
71. M. Azzouzi, N. P. Gallop, F. Eisner, J. Yan, X. Zheng, H. Cha, Q. He, Z. Fei, M. Heeney, A. A. Bakulin and J. Nelson, *Energy & Environmental Science*, 2022, **15**, 1256-1270.
72. Marcusfit, https://github.com/junyannj/Marcusfit, 2025.
73. T. M. Burke, S. Sweetnam, K. Vandewal and M. D. McGehee, *Advanced Energy Materials*, 2015, **5**, 1500123.
74. A. Troisi, *Chemical Society Reviews*, 2011, **40**, 2347-2358.
75. M. Bixon, J. Jortner and J. W. Verhoeven, *Journal of the American Chemical Society*, 1994, **116**, 7349-7355.
76. M. Saladina, C. Wöpke, C. Göhler, I. Ramirez, O. Gerdes, C. Liu, N. Li, T. Heumüller, C. J. Brabec, K. Walzer, M. Pfeiffer and C. Deibel, *Physical Review Letters*, 2023, **130**, 236403.
77. D. de Sa Pereira, C. Menelaou, A. Danos, C. Marian and A. P. Monkman, *The Journal of Physical Chemistry Letters*, 2019, **10**, 3205-3211.
78. A. Devižis, J. De Jonghe-Risse, R. Hany, F. Nüesch, S. Jenatsch, V. Gulbinas and J.-E. Moser, *Journal of the American Chemical Society*, 2015, **137**, 8192-8198.

View Article Online
DOI: 10.1039/D5EL00216H

79. S. Mahadevan, T. Liu, S. M. Pratik, Y. Li, H. Y. Ho, S. Ouyang, X. Lu, H.-L. Yip, P. C. Y. Chow, J.-L. Brédas, V. Coropceanu, S. K. So and S.-W. Tsang, *Nature Communications*, 2024, **15**, 2393.
80. P. Wan, X. Chen, Q. Liu, S. Mahadevan, M. Guo, J. Qiu, X. Sun, S.-W. Tsang, M. Zhang, Y. Li and S. Chen, *The Journal of Physical Chemistry Letters*, 2021, **12**, 10595-10602.
81. W. Liptay, in *Excited states*, Elsevier, 1974, vol. 1, pp. 129-229.
82. L. Sebastian, G. Weiser and H. Bässler, *Chemical Physics*, 1981, **61**, 125-135.
83. C.-q. Cao, W. Long and H. Cao, *Physics Letters A*, 1997, **232**, 15-24.
84. J. S. Müller, M. Comí, F. Eisner, M. Azzouzi, D. Herrera Ruiz, J. Yan, S. S. Attar, M. Al-Hashimi and J. Nelson, *ACS Energy Letters*, 2023, **8**, 3387-3397.
85. H. Wu, H. Lu, Y. Li, X. Zhou, G. Zhou, H. Pan, H. Wu, X. Feng, F. Liu, K. Vandewal, W. Tress, Z. Ma, Z. Bo and Z. Tang, *Nature Communications*, 2024, **15**, 2693.

View Article Online
DOI: 10.1039/D5EL00216H

Data availability

All the data supporting the current study are available in its Supplementary Material files or from the corresponding authors upon reasonable request. The code is available via GitHub: https://github.com/junyannj/Marcusfit.